The transition between square-wave and pseudo-plateau bursting

Ragheb Hasan

Supervisors: Professor Hinke Osinga
A/Professor Vivien Kirk

A thesis submitted in fulfilment of the requirements for the degree of Master of Science in Applied Mathematics,
Department of Mathematics,
The University of Auckland, 2013.

Abstract

Electrically excitable cells such as neurons may exhibit different types of bursting activities due to a difference in timescales between changes in electrical potential across the cell membrane and changes in concentration of ions inside the cells. Some of these bursting activities can be observed in mathematical models with multiple timescales. We focus on two types of bursting patterns that appear to be very similar in the observed experimental data but are different in terms of the mathematical mechanism by which they are generated; these are so-called square-wave and pseudo-plateau bursting.

In this thesis, we study the mathematical structure of square-wave and pseudo-plateau bursting patterns in a polynomial system of ordinary differential equations with one slow and two fast variables. We use the technique of freezing the single slow variable and relating the resulting bifurcation diagram of the fast subsystem to the dynamics of the full system. This polynomial system can exhibit both types of bursting, depending on the choice of parameters. We are interested in a continuous deformation from square-wave to pseudo-plateau bursting, which we study by numerical continuation. We find that a direct transition between the two bursting patterns through a single connected family can be obtained via a variation of a single bifurcation parameter. As the pseudo-plateau bursting pattern transforms into the square-wave bursting pattern, a transitional bursting pattern arises. This transitional bursting pattern can be viewed as a mix between square-wave and pseudo-plateau bursting.

Based on our understanding gained from studying the polynomial model, we propose precise definitions for square-wave, pseudo-plateau and transitional bursting patterns in generic systems with one slow and two fast variables. Our classifications of the different bursting patterns depend mainly on the underlying bifurcation diagram of the fast subsystem, the location

of the nullcline of the slow variable and the timescale ratio between the variables.

Acknowledgements

Firstly, I would like to express my deepest appreciation and gratitude to my lovely supervisors Vivien Kirk and Hinke Osinga for their exceptional support, guidance and patience. I have gained enormous knowledge from them and it was a huge privilege to work under their supervision. I am also grateful that I had the opportunity to discuss some of my work with other great researchers like Jonathan Rubin, Arthur Sherman and Krasimira Tsaneva-Atanasova during their visits to Auckland. I would also like to thank all senior students who guided me and shared their experiences with me.

Secondly, I want to acknowledge the great support from my wonderful family from overseas, especially my parents and older brother. I would also like to thank all of my friends who showed their support throughout my period of study.

Contents

Abstract **i**

Acknowledgements **iii**

List of Figures **viii**

List of Tables **x**

1 Introduction and mathematical background **1**

1.1 Introduction 1

1.2 Mathematical Background 3

1.3 Aims and outline of the thesis 6

2 Fast-slow analysis of the polynomial model **9**

2.1 Introducing the model 9

2.2 Bifurcation analysis of the fast subsystem 10

2.3 Analysis of the full system 21

3 Characterisation of the different bursting patterns **31**

3.1 Square-wave bursting 32

3.2 Pseudo-plateau bursting 36

3.3 The transitional bursting patterns 41

4 Moving the nullcline of the slow variable **47**

5 Moving the curve of homoclinic bifurcations of the fast subsystem **55**

6 Conclusions **61**

6.1 Summary 61

6.2 Directions for future research 63

Appendix A **65**

References **67**

List of Figures

1.1 Schematic examples of square-wave and pseudo-plateau bursting 2
1.2 An example of a bursting orbit overlaid on the bifurcation diagram of the fast subsystem, as well as the corresponding time series 4

2.1 Bifurcation diagrams of the fast subsystem of the polynomial model for the cases $s = -1.61$ and $s = -2.38$ 11
2.2 Two-parameter bifurcation set of the fast subsystem of the polynomial model . 13
2.3 Two-parameter bifurcation set of the fast subsystem near the degenerate cusp point with representative phase portraits near that point 14
2.4 The sign of the quantity γ along the curve of Hopf bifurcations of the fast subsystem 16
2.5 Belyakov point in the two-parameter plane of the fast subsystem corresponds to the intersection of the curve of homoclinic bifurcations with the curve where the saddle quantity is zero 18
2.6 An enlargement of part of the two-parameter set of the fast subsystem showing the absence of SNIC bifurcations 18
2.7 Representative bifurcation diagrams of the fast subsystem for six qualitatively different s-dependent regions 20
2.8 The location of the z-nullcline for $s = -1.61$ and $s = -2.15$, superimposed on the bifurcation diagram of the corresponding fast subsystem 22
2.9 Bursting patterns in the full system of the polynomial model for two choices of s and two choices of ϵ 23

2.10 Bifurcation diagram of the full system, with s varying and $\epsilon = 0.01$ 25
2.11 Bifurcation diagram of the full system with s varying and $\epsilon = 0.005$ 26
2.12 The transition between square-wave and pseudo-plateau bursting in the full system, with s is varying and $\epsilon = 0.001$ 28

3.1 A typical example of square-wave bursting overlaid on the corresponding bifurcation diagram of the fast subsystem 33
3.2 A typical example of pseudo-plateau bursting overlaid on the corresponding bifurcation diagram of the fast subsystem 38
3.3 A typical example of the standard transitional bursting pattern bursting overlaid on the corresponding bifurcation diagram of the fast subsystem 42

4.1 The locus of equilibrium points of the full system in relation to the bifurcation curves of the fast subsystem in the (z, s)-plane 48
4.2 Bifurcation diagram of the full system after changing the location of the z-nullcline, with s varying and $\epsilon = 0.001$ 49
4.3 The transition between square-wave and pseudo-plateau bursting in the full system after changing the location of the z-nullcline, with s varying and $\epsilon = 0.0001$ 51

5.1 Two-parameter bifurcation set of the fast subsystem for the new value of a . . . 56
5.2 Bifurcation diagram of the full system for the new value of a, with s varying and $\epsilon = 0.001$ 57
5.3 The transition from square-wave to pseudo-plateau bursting in the full system for the new value of a 58

A.1 Two-parameter bifurcation set of the fast subsystem of the polynomial model with $\phi = 0.6$ 66

List of Tables

2.1 Qualitatively different s-dependent regions of the fast subsystem 19

Chapter 1

Introduction and mathematical background

1.1 Introduction

Many physiological phenomena have the property that some processes evolve much faster than others. For example, in electrically excitable cells, it is observed that changes in electrical potential across the cell membrane occur much more quickly than changes in concentration of ions, such as calcium ions, within the cytoplasm. This property of physiological systems can be captured by the construction of mathematical models with multiple timescales, where some variables change more rapidly than others. The physiological phenomena associated with mathematical models with multiple timescales can be very complicated. We focus on two types of complicated oscillations that occur in physiological models, namely, so-called square-wave (plateau) [25] and pseudo-plateau [27] bursting.

Bursting is a complex oscillatory waveform typically found in electrically excitable cells such as neurons and endocrine cells, and it is characterised by alternating periods of fast spiking oscillations in the active (depolarized) phase and a quiescence in the silent (repolarized) phase [27, 33, 34]. Figure 1.1 shows schematic examples of both square-wave and pseudo-plateau bursting. Here, x represents the voltage across the cell membrane of an excitable cell,

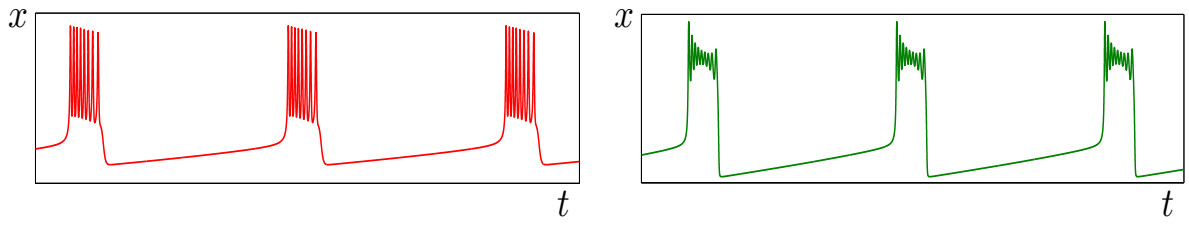

(a) (b)

Figure 1.1: Schematic examples of square-wave and pseudo-plateau bursting. Here, x represents the voltage across the cell membrane of some type of an excitable cell, and t represents time. Panel (a) shows square-wave bursting where the spike amplitudes are relatively large and consistent in size, and panel (b) shows pseudo-plateau bursting where the spike amplitudes are relatively small and variable in size.

and t represents time. A time series such as that illustrated in Figure 1.1(a) is typical of square-wave bursting; the spike amplitudes are relatively large and consistent in size. A time series like that shown in Figure 1.1(b) is typical of pseudo-plateau bursting; the spike amplitudes are relatively small and variable in size. Square-wave and pseudo-plateau bursting are thought to be associated with different physiological processes in electrically excitable cells. For instance, the large-amplitude, short-duration spikes characteristic in square-wave bursting are effective at evoking neurotransmitter release in neural cells [31]. In contrast, the small-amplitude spikes characteristic in pseudo-plateau bursting produce an elevated average calcium (Ca^{2+}) concentration in endocrine cells [31]. We are interested in studying square-wave and pseudo-plateau bursting patterns because the associated time series are broadly similar, but the underlying mathematical mechanisms that generate the bursts are thought to be quite distinct.

In this thesis, we investigate in detail the mathematical mechanisms underlying square-wave and pseudo-plateau bursting patterns, and characterise the differences between these two patterns in terms of these mathematical mechanisms.

1.2 Mathematical Background

We are interested in systems of ordinary differential equations that have the form:

$$\begin{cases} \dot{x} = & f(x, y, z, s), \\ \dot{y} = & g(x, y, z, s), \\ \dot{z} = & \epsilon h(x, y, z, s), \end{cases} \tag{1.1}$$

where x and y are fast variables, z is a slow variable, s and ϵ are parameters, and $0 < \epsilon \ll 1$. Assuming that the functions f, g and h are of the same order, we can regard ϵ as the ratio between slow and fast timescales.

The core technique that we will use to analyse systems of this form exploits the separation of timescales inherent in the system. Specifically, to investigate the behaviour of solutions at a fixed value of s, we first freeze the slow variable z, by taking the limit of (1.1) as $\epsilon \to 0$. System (1.1) then effectively becomes a two-dimensional system

$$\begin{cases} \dot{x} = & f(x, y, z, s), \\ \dot{y} = & g(x, y, z, s), \end{cases} \tag{1.2}$$

where z is now a parameter since $\dfrac{dz}{dt} = 0$ in the singular limit of ϵ. We call (1.2) the fast subsystem of system (1.1). This fast subsystem is organised by steady-state solutions and periodic solutions. The next step is to plot the bifurcation diagram of (1.2) with z as the bifurcation parameter, and s still fixed. Without any loss of generality, we plot the curves of steady-state solutions of the fast subsystem, and the maximum and minimum x-values of the periodic orbits of the fast subsystem in the (z, x)-plane. The z-nullcline of system (1.1) is a two-dimensional surface, given by $h(x, y, z, s) = 0$. However, we can represent the z-nullcline as a one-dimensional curve in the (z, x)-plane. The following step is to superimpose the z-nullcline curve on the bifurcation diagram of the fast subsystem. Finally, we will plot the solutions of (1.1) for fixed small $\epsilon > 0$, fixed s, and x, y, z allowed to vary, on the same figure. By comparing the solutions to (1.1) with the bifurcation diagram of (1.2), we are able to distinguish between the different types of solutions and understand the mechanism by which each type occurs. This technique

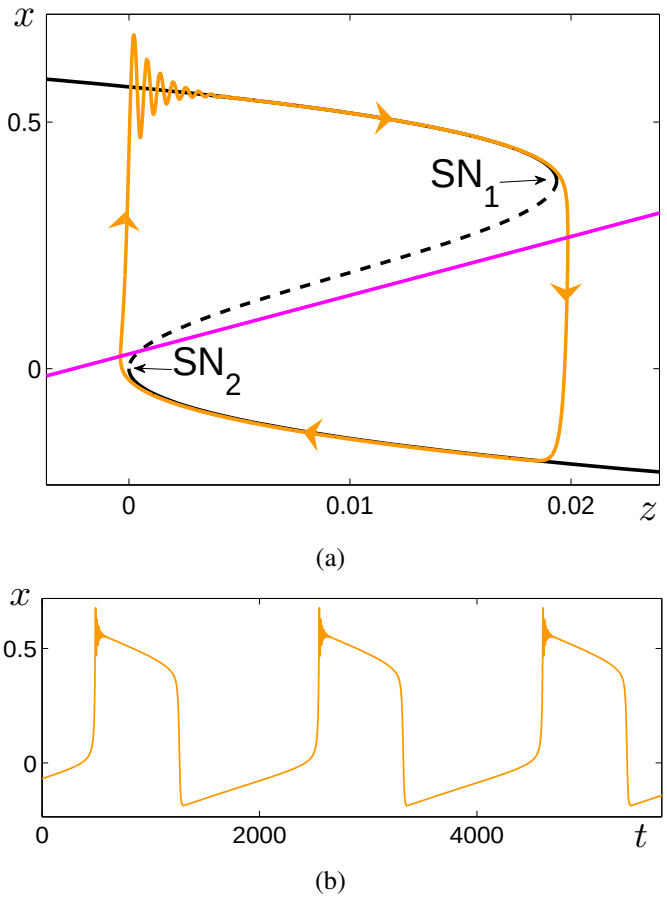

Figure 1.2: A bursting orbit (orange) of system (2.1) from Chapter 2, which has the form of (1.1). Panel (a) shows the bursting orbit overlaid on the corresponding bifurcation diagram of the fast subsystem. Here, x is a fast variable and z is the slow variable. Black curves denote the steady-state solutions of the fast subsystem for varying values of the frozen variable z; solid when stable and dashed when unstable. The saddle-node bifurcations of the fast subsystem are labelled SN_1 and SN_2. The z-nullcline is represented by the magenta line. Panel (b) shows the corresponding time series of x, where t represents time. Values of parameters are as follows: $s = -1.4$, $\epsilon = 0.005$, $a = 0.5$, $b = 1$, $\phi = 1$, $a_1 = -0.012$, $b_1 = -0.0005$, and $k = 0.2$.

also allows us to explain the time series of x by relating it to the corresponding solutions overlaid on the bifurcation diagram of the fast subsystem in the (z, x)-plane.

Figure 1.2 shows an example of a bursting orbit for a model of the form of (1.1); this orbit

is obtained using system (2.1), which will be introduced in Chapter 2. Here, the variable x is fast, z is slow, and the parameters s and ϵ are fixed. Panel (a) shows the bursting orbit overlaid on the corresponding bifurcation diagram of the fast subsystem in the (z, x)-plane; the corresponding time series of x is shown in panel (b). In panel (a), the black curves denote the steady-state solutions of the fast subsystem for varying values of the frozen variable z; solid when stable and dashed when unstable. There are two saddle-node bifurcations of the fast subsystem, labelled SN_1 and SN_2. The equation of the z-nullcline surface in system (2.1) does not depend on y. Hence, we can think of it as one-dimensional object in the (z, x)-plane; this object is represented by the magenta line superimposed on the bifurcation diagram of the fast subsystem. The attracting trajectory of the full system, shown in orange, is overlaid on the bifurcation diagram of the fast subsystem.

We can understand the time series of x by comparing it to the corresponding trajectory overlaid on the bifurcation diagram of the fast subsystem in Figure 1.2. In particular, the trajectory at $t = 0$ in panel (b) corresponds to the trajectory on the lower branch of attracting (stable) steady states of the fast subsystem in panel (a). As t increases in panel (b), the corresponding trajectory in panel (a) jumps up at SN_2 where the lower branch of attracting steady states loses stability. Then, the trajectory develops a few spikes around an upper branch of attracting steady states with complex eigenvalues (spiral sinks) of the fast subsystem. Eventually, the trajectory converges to that upper branch of attracting steady states, then jumps back down at SN_1 to the lower branch of attracting steady states, and the bursting orbit repeats. Observe how the trajectory moves to the right in the region above the z-nullcline, and to the left on the other side of the z-nullcline. The active and silent phases of the burst in panel (b) correspond to the trajectory overlaid on the upper and lower branches of steady states of the fast subsystem in panel (a), respectively. This technique enables us to use the information obtained from the fast subsystem and the z-nullcline to describe the behaviour of the full system. Moreover, this technique helps us to understand the mathematical mechanism by which a particular time series of x is generated.

The procedure discussed above helps to explain the origin of complicated dynamics for fixed values of s, the main bifurcation parameter in the original system (1.1). If s changes, the bifurcation structure of the fast subsystem can also change, with corresponding changes in

the dynamics of the full system. For example, square-wave bursting is associated with certain types of structure of the underlying bifurcation diagram of the fast subsystem that occur for certain fixed values of s. Likewise, pseudo-plateau bursting in the full system requires other types of structure of the underlying bifurcation diagram of the fast subsystem that correspond to other fixed values of s. We aim to use this information to construct a one-parameter family of ordinary differential equations that exhibit square-wave bursting for one interval of parameter values and pseudo-plateau bursting for another interval; detailed study of such a family will then give information about the transition from one bursting pattern to the other.

The technique of freezing a slow variable and using the underlying bifurcation diagram of the fast subsystem to explain the dynamics of the original system has been used by [13, 24, 26, 31, 32]. This technique works well in the case that the system has a single global slow variable, and the separation of timescales is sufficiently large (i.e., ϵ is sufficiently small in system (1.1)). In this case, the technique is known to be equivalent to methods from geometric singular perturbation theory (GSPT) [14, 15], but we do not explore GSPT in more detail in this thesis. The main advantage of this reduction technique is that we can simplify the system and use the resulting bifurcation diagram of the reduced fast subsystem as a guide to understand the complex behaviour of the full system.

1.3 Aims and outline of the thesis

In this thesis, we aim to find a simple system of ordinary differential equations in which a direct transition between square-wave and pseudo-plateau bursting is obtained by varying a single bifurcation parameter. We wish to use this family in order to understand how the two bursting patterns are related. In Chapter 2, we use a generic polynomial model that is in the form of (1.1). In particular, we use system (2.1), which was introduced in [32]. This chapter starts with a presentation of the equations of the polynomial model, followed by the results of analysing both the fast subsystem and the full system. Chapter 3 proposes characterising criteria and conditions for square-wave, pseudo-plateau and transitional bursting patterns for all systems with one slow and two fast variables. This characterisation helps us to distinguish between the different bursting patterns and understand the underlying mathematical mechanism by which a given

bursting pattern occurs. Using these criteria and conditions, we look for a cleaner transition between square-wave and pseudo-plateau bursting in the polynomial model (2.1). In Chapter 4, we examine the effect of the location of the z-nullcline on the transition between square-wave and pseudo-plateau bursting in the polynomial model. Chapter 5 presents the transition between the two bursting patterns in the polynomial model after moving the loci of some of the bifurcations in the two-parameter plane of the fast subsystem. Chapter 6 summarises the main results of the study and discusses possible directions for future work. XPPAUT [6] and MATLAB [18] are the main numerical tools used in the study.

Chapter 2

Fast-slow analysis of the polynomial model

In this chapter, we use a polynomial system of ordinary differential equations to find a transition between square-wave and pseudo-plateau bursting. Since we use the technique of freezing the slow variable as a main ingredient in identifying the different types of bursting, we commence with a bifurcation analysis of the fast subsystem. Then we relate the different behaviour of the full system to the associated bifurcation structures of the fast subsystem. Lastly, we look for a direct transition between the two bursting patterns in the full system by changing only one parameter.

2.1 Introducing the model

We use the polynomial model introduced by Tsaneva-Atanasova et al., in [32], given by the following system of ordinary differential equations:

$$\begin{cases} \dot{x} = & sax^3 - sx^2 - y - bz, \\ \dot{y} = & \phi(x^2 - y), \\ \dot{z} = & \epsilon(sa_1x + b_1 - kz), \end{cases} \tag{2.1}$$

where $x, y, z \in \mathbb{R}$, are the variables of the system, while s, a, b, a_1, b_1, k, ϕ and ϵ are constants. For the purposes of this chapter, we follow [32] and set $\phi = 1$ and choose ϵ to be small (i.e.,

$0 < \epsilon \ll 1$). We also choose $a = 0.5$, $b = 1$, $a_1 = -0.1$, $b_1 = -0.0279$ and $k = 0.2$, the same values that were used in [32] and [24] except that in those papers b_1 was varied. Our choice of a_1 and b_1 will be discussed further in Section 2.3. The main bifurcation parameter of our study is s; we are interested mostly in $s \in (-3, -1)$. Since s, a and b are all of order one while a_1, b_1 and k are smaller, our choice of ϕ and ϵ makes the evolution of z much slower than that of x and y. Therefore, we can regard x and y as fast variables and z as a slow variable.

2.2 Bifurcation analysis of the fast subsystem

The fast subsystem of the model is obtained by taking the singular limit of system (2.1). Hence, the fast subsystem is:

$$\begin{cases} \dot{x} = & sax^3 - sx^2 - y - bz, \\ \dot{y} = & \phi(x^2 - y), \end{cases} \tag{2.2}$$

where z is constant and can be treated as a bifurcation parameter.

Steady-state solutions of the fast subsystem occur at the intersection of the x-nullcline and y-nullcline of (2.2), and correspond to the roots of the following cubic equation:

$$sax^3 - (s+1)x^2 - bz = 0. \tag{2.3}$$

It is evident that the locus of these steady-state solutions depends on the parameter s and the frozen variable z. Figure 2.1 shows two bifurcation diagrams for the fast subsystem in the (z, x)-plane; panel (a) has $s = -1.61$, panel (b) has $s = -2.38$. In both cases, the curve of steady states starts from the top left of the figure with a branch of stable steady states that loses stability after crossing a Hopf bifurcation (HB).

Figure 2.1(a) shows the case for $s = -1.61$, where the Hopf bifurcation is supercritical and produces a branch of stable periodic orbits. In Figure 2.1(b), where $s = -2.38$, the Hopf bifurcation is subcritical and generates a branch of unstable periodic orbits. In both cases, the unstable branch of steady states undergoes a saddle-node bifurcation (SN_1), and converts to a saddle branch. The curve of steady-state solutions changes direction again through another saddle-node bifurcation (SN_2), and regains its stability. In each case, the branch of periodic

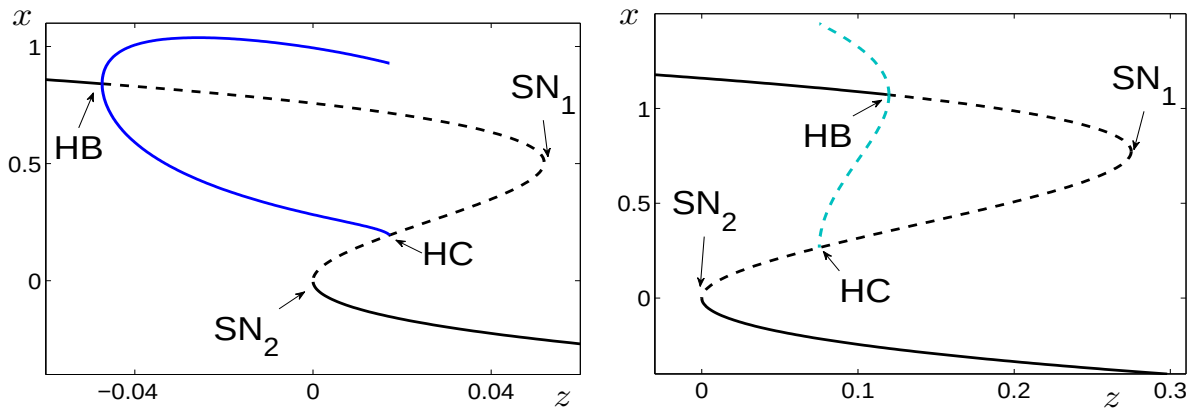

Figure 2.1: Bifurcation diagrams of the fast subsystem (2.2) in the $(z,\ x)$-plane, for the two cases (a) $s = -1.61$ and (b) $s = -2.38$. Here z acts as a bifurcation parameter, and $a = 0.5$, $b = 1$, $\phi = 1$. The black curve represents steady-state solutions; solid when stable, dashed when unstable. Blue curves indicate the maximum and minimum x-values of the periodic orbits; solid dark-blue when stable, dashed light-blue when unstable. HB−Hopf bifurcation; SN−saddle-node bifurcation; HC−homoclinic bifurcation.

orbits terminates at a homoclinic bifurcation (HC), where the periodic orbit of the fast subsystem collides with a saddle point on the middle branch of steady states.

It is useful to locate the bifurcations of the fast subsystem in the $(z,\ s)$-parameter plane; this enables us to understand the transition from supercritical to subcritical Hopf bifurcations as s varies. A two-parameter bifurcation analysis of the fast subsystem of the model has also been performed, to some extent, in [4, 24, 32].

We start with finding some of the bifurcations analytically in terms of the parameters s, a, b and ϕ, assuming that s is negative, and a, b and ϕ are all positive. We further assume that $\phi < \dfrac{2}{3a}$.

Saddle-node bifurcations in two-dimensional systems are characterized by a zero eigenvalue of the Jacobian matrix at the equilibria. It is straightforward to show that saddle-node bifurcations of the fast subsystem occur at

$$z_{SN_1} = \frac{sax_{SN_1}^3 - (s+1)x_{SN_1}^2}{b}, \text{ and } z_{SN_2} = 0, \tag{2.4}$$

where

$$x_{SN_1} = \frac{2(s+1)}{3sa}.$$

Therefore, there are two saddle-node bifurcations for all negative values of s except for $s = -1$ where there is only one.

Hopf bifurcations in two-dimensional systems are characterized by a zero trace and a positive determinant at the Jacobian matrix. Our calculations show that for each $s \leqslant -3\phi a$ there exists at least one Hopf bifurcation of the fast subsystem, at

$$z_{HB} = \frac{sax_{HB}^3 - (s+1)x_{HB}^2}{b}, \tag{2.5}$$

where

$$x_{HB} = \frac{s \pm \sqrt{s^2 + 3\phi sa}}{3sa} \text{ for } s > \frac{4}{3a\phi - 4}, \tag{2.6}$$

$$x_{HB} = \frac{s - \sqrt{s^2 + 3\phi sa}}{3sa} \text{ for } s \leqslant \frac{4}{3a\phi - 4}. \tag{2.7}$$

Therefore, for our choice of parameters, Hopf bifurcations exist only for $s \leqslant -1.5$. Also, for our choice of parameters, there are two co-existing Hopf bifurcations corresponding to (2.6), and they exist for $-1.6 < s \leqslant -1.5$; and there is only one Hopf bifurcation corresponding to (2.7), and it exists for $s \leqslant -1.6$.

The loci in the (z, s)-plane of other bifurcations of the fast subsystem, that is, homoclinic bifurcations and fold bifurcations of periodic orbits, were computed using the continuation tool of XPPAUT [6]. The approximate locus of homoclinic bifurcations was calculated by following periodic orbits of a fixed high period in XPPAUT, specifically, $T = 4000$.

Figure 2.2 shows the different bifurcation curves for the fast subsystem in the (z, s)-parameter plane. The black curves are curves of the saddle-node bifurcations. The curve of Hopf bifurcations (HB), the curve of homoclinic bifurcations (HC) and the curve of fold bifurcations of periodic orbits (FPO) are the red, green and blue curves, respectively.

By inspection of Figure 2.2, we identify four codimension-two bifurcations in the fast subsystem, as denoted with the black dots. The first identified codimension-two bifurcation is a

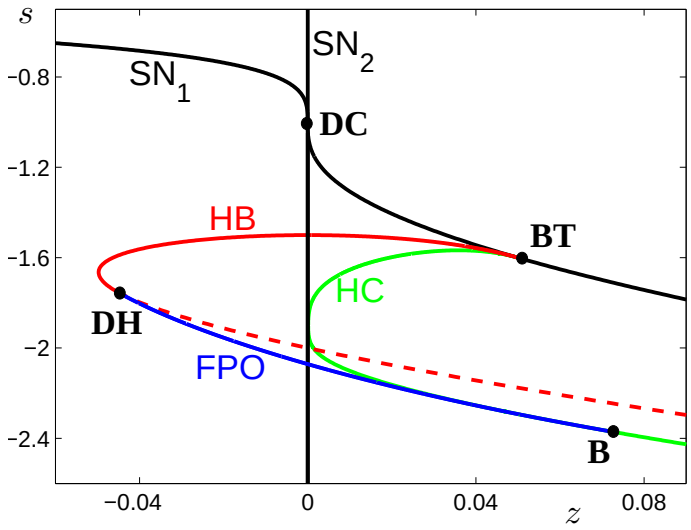

Figure 2.2: Two-parameter bifurcation set of the fast subsystem (2.2). Here z and s are bifurcation parameters, and $a = 0.5$, $b = 1$, $\phi = 1$. The black curves labelled SN_1 and SN_2 represent the loci of saddle-node bifurcations. The red curve labelled HB marks the locus of Hopf bifurcations; solid when supercritical and dashed when subcritical. The curve of homoclinic bifurcations (HC) and the curve of fold bifurcations of periodic orbits (FPO) correspond to the green and blue curves, respectively. Codimension-two bifurcation points are labelled with black dots: DC−degenerate cusp point; BT−Bogdanov-Takens point; DH−degenerate Hopf point; B−Belyakov point.

degenerate cusp point (DC). In general, a cusp bifurcation can occur on a curve of saddle-node bifurcations, usually when two such curves come together at a point. In our case, the point labelled DC in Figure 2.2 occurs as two saddle-node curves cross each other, so it does not appear to be a generic cusp. We have found the loci of both saddle-node bifurcations analytically (2.4), and it is straightforward to show that they intersect at $(z, s) = (0, -1)$ for all values of a, b, and ϕ.

The normal form for a nondegenerate cusp point is given in [11, 12, 17] as the following:

$$\dot{x} = \pm x^3 + \alpha_1 x - \alpha_2 + O(x^4),$$

where α_1 and α_2 are coefficients. A straightforward centre manifold calculation in our model shows that, at the cusp point marked DC in Figure 2.2, the linear term is missing from the

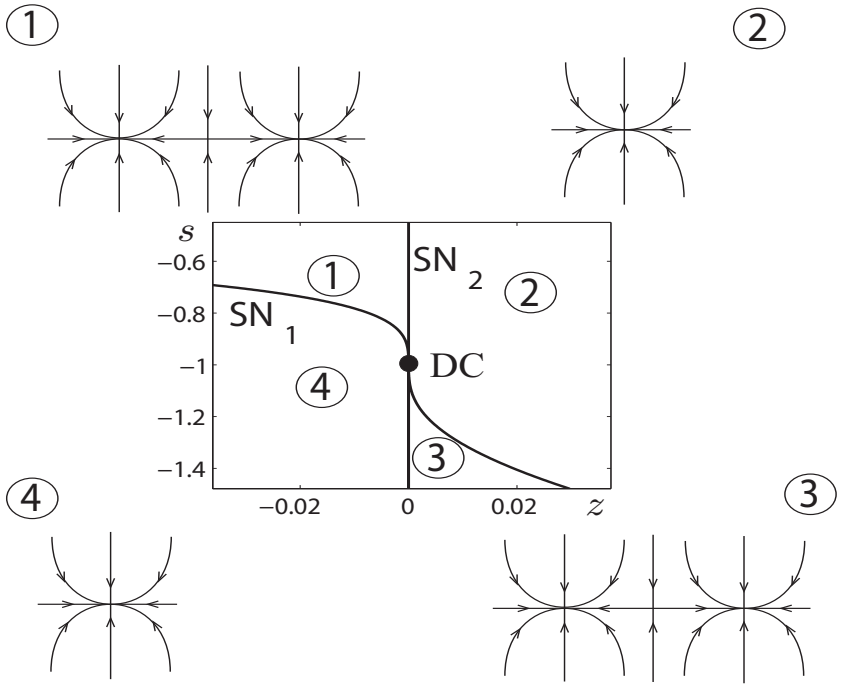

Figure 2.3: Two-parameter bifurcation set of the fast subsystem (2.2), near the degenerate cusp point labelled DC in Figure 2.2, with representative phase portraits near that point. Values of other parameters are as for Figure 2.2. SN−saddle-node bifurcation; DC−degenerate cusp point.

normal form (i.e., $\alpha_1 = 0$) and is replaced with a quadratic term in x. This results in the curves of saddle-node bifurcations persisting even after passing through the degenerate cusp point, unlike the case for a nondegenerate cusp point. Hence, the cusp point at $(z, s) = (0, -1)$ is degenerate.

Figure 2.3 shows the degenerate cusp point of the fast subsystem in the two-parameter set and the corresponding phase portraits for the regions near the point. In regions 1 and 3, there are a saddle equilibrium point and two stable equilibrium points. In regions 2 and 4, there is only one equilibrium point and it is stable.

The second codimension-two bifurcation is a Bogdanov-Takens point (BT). In planar systems, Bogdanov-Takens bifurcations occur when the Jacobian matrix can be reduced to a zero Jordan block of order 2, that is, the Jacobian matrix has a zero eigenvalue of algebraic multiplicity two and geometric multiplicity one [12, 17]:

$$\begin{pmatrix} 0 & 1 \\ 0 & 0 \end{pmatrix}.$$

This Jacobian matrix has a zero trace and a zero determinant. It is known that generically a saddle-node bifurcation (determinant zero equilibrium) and a Hopf bifurcation (trace zero equilibrium) collide at a Bogdanov-Takens point [10, 12, 17]. In our model, this occurs at

$$(z, s) = \left(\frac{\beta a(\frac{2(\beta+1)}{3\beta a})^3 - (\beta+1)(\frac{2(\beta+1)}{3\beta a})^2}{b}, \beta \right),$$

where

$$\beta = \frac{4}{3a\phi - 4}.$$

Therefore, for our choice of parameters, a Bogdanov-Takens point exists at $(z, s) = (0.05, -1.6)$. Theory also states that a curve of homoclinic bifurcations emerges from a Bogdanov-Takens point [10, 12, 17]. Figure 2.2 shows that the curves of Hopf bifurcations and homoclinic bifurcations emerge from the Bogdanov-Takens point, and a curve of saddle-node bifurcations (SN_1) passes through that point, just as expected.

The third considered codimension-two bifurcation is a degenerate Hopf point (DH) which is a point on a Hopf bifurcation curve where the Hopf bifurcation changes its criticality. Criticality of a Hopf bifurcation can be determined by the sign of the first Lyaponouv coefficient [12, 16, 17]; if the first Lyaponouv coefficient is negative, the Hopf bifurcation will be supercritical, while if the first Lyaponouv coefficient is positive, the Hopf bifurcation will be subcritical. The calculation of the first Lyaponouv coefficient, in general, requires a lengthy process. However, according to [12, 16, 32], if we have a two-dimensional system in the form:

$$\begin{aligned} \dot{x} &= \quad F(x) - y, \\ \dot{y} &= \mu(G(x) - y), \end{aligned}$$

then we can find the sign of the first Lyaponouv coefficient by finding the sign of the quantity γ

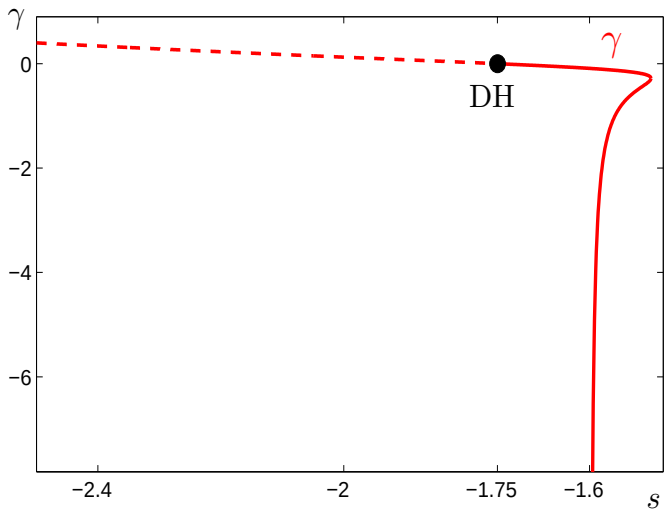

Figure 2.4: The criticality of Hopf bifurcations in the fast subsystem (2.2), with parameter values as for Figure 2.2, is determined by the sign of the quantity γ. The red curve shows the value of γ along the curve of Hopf bifurcations; solid when the corresponding Hopf bifurcation is supercritical; dashed when subcritical. The degenerate Hopf point (DH) is denoted by the black dot.

at the Hopf bifurcation, where γ is defined by

$$\gamma(x_{HB}) = \frac{1}{16}\left[F''' + F''\left(\frac{F'' - G''}{G' - \mu}\right)\right].$$

In our model,

$$\gamma(x_{HB}) = \frac{1}{16}\left[6sa + (6sax_{HB} - 2s)\left(\frac{6sax_{HB} - 2s - 2}{2x_{HB} - \phi}\right)\right], \tag{2.8}$$

where x_{HB} is determined by formulae (2.6)-(2.7).

Figure 2.4 shows the corresponding values of γ for our choice of parameters, calculated using (2.8). The figure shows that the co-existent Hopf bifurcations for $-1.6 < s \leqslant -1.5$ always have a negative first Lyaponouv coefficient and, hence, are always supercritical. The figure also shows that the Hopf bifurcation has a negative first Lyaponouv coefficient for the range $-1.75 < s \leqslant -1.6$, and has a positive first Lyaponouv coefficient for $s < -1.75$.

Therefore, there is a degenerate Hopf point (DH) at $(z, s) \approx (-0.0454, -1.75)$ where the first Lyaponouv coefficient is zero [9, 12, 17]. Figure 2.2 shows how a degenerate Hopf point also gives rise to a fold bifurcation of periodic orbits (FPO).

The fourth codimension-two bifurcation of the fast subsystem is a Belyakov point (B), which occurs when the saddle point involved in a homoclinic bifurcation has a saddle quantity (δ) of zero, i.e., the sum of the leading eigenvalues of the saddle point is zero [2, 7, 12]. A consequence of the change in sign of δ is that the branch of periodic orbits terminating at the homoclinic bifurcation changes stability [2, 17]. In a two-dimensional system, the curve where the saddle quantity is zero (δ_0) is characterised by a zero trace and a negative determinant of the Jacobian matrix. Hence, it is a continuation of the Hopf bifurcation curve (since the Hopf bifurcation corresponds to a zero trace and a positive determinant of the Jacobian matrix). Therefore, the curve δ_0 where the saddle quantity is zero in the fast subsystem is defined by the following formula:

$$z_{\delta_0} = \frac{sax_{\delta_0}^3 - (s+1)x_{\delta_0}^2}{b}, \tag{2.9}$$

where

$$x_{\delta_0} = \frac{s + \sqrt{s^2 + 3\phi sa}}{3sa}, \text{for } s < \frac{4}{3a\phi - 4}.$$

Figure 2.5 shows the curve where the saddle quantity is zero (δ_0, cyan), as well as the locus of homoclinic bifurcations (HC, green) in the (z, s)-parameter plane. The Belyakov point occurs at the intersection between the two curves; namely at $(z, s) \approx (0.0725, -2.37)$. The figure illustrates that the Belyakov point also puts an end to the curve of fold bifurcations of periodic orbits (FPO). The figure also shows that the curve of Hopf bifurcations (HB) is a continuation of the curve where the saddle quantity is zero.

We also investigate the existence of saddle-node on invariant circle (SNIC) bifurcations, which occur when a periodic orbit collides with a saddle-node point in the phase space creating an invariant circle [5, 8, 12]. Figure 2.2 appears to show that the second saddle-node bifurcation curve (SN_2) and the homoclinic bifurcation curve (HC) intersect at some point, establishing a SNIC bifurcation. However, an enlarged section of the two-parameter bifurcation set is shown in Figure 2.6, in which it can be seen that these curves actually do not intersect. Hence, SNIC

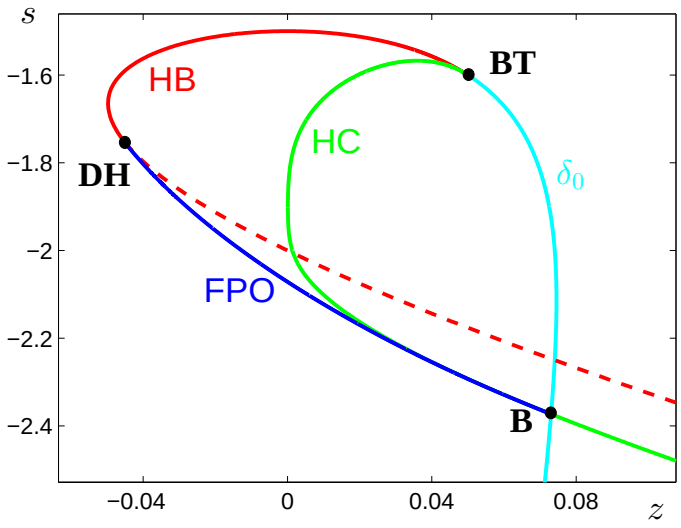

Figure 2.5: The curve of homoclinic bifurcations (HC, green) and the curve where the saddle quantity is zero (δ_0, cyan) intersect at the Belyakov point (B) in the (z, s)-parameter plane of the fast subsystem (2.2). Values of parameters are as for Figure 2.2. The curve of saddle quantity zero and the curve of Hopf bifurcations (HB, red) join smoothly at Bogdanov-Takens point (BT) since both curves represent steady-state solutions with trace zero. The curve of fold bifurcations of periodic orbits (FPO, blue) ends at the Belyakov point. Other line styles and labels are as for Figure 2.2.

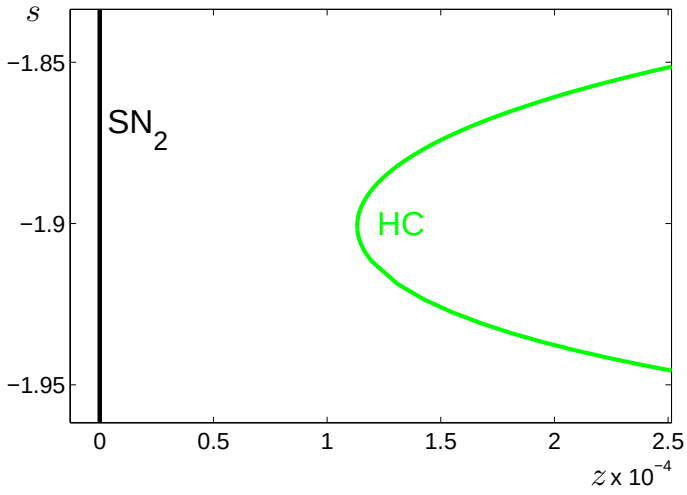

Figure 2.6: An enlargement of part of Figure 2.2 showing the absence of SNIC bifurcations.

bifurcations do not appear in the fast subsystem for this choice of parameters.

Now we identify qualitatively different s-dependent regions of the fast subsystem. Table 2.1 shows the ranges of s for the six identified regions, and Figure 2.7 shows typical bifurcation diagrams for each region. Figure 2.7(a) shows a typical case for the first region ($s = -1.4$), where only saddle-node bifurcations occur. The second region (Figure 2.7(b)) sees the emergence of two co-existing Hopf bifurcations creating an interconnected family of stable periodic orbits. The third region (Figure 2.7(c)) gives rise to two homoclinic bifurcations breaking up the interconnected family of periodic orbits into two separate families of stable periodic orbits. Figure 2.7(d) shows a standard case for the fourth region where there is only one supercritical Hopf bifurcation and one homoclinic bifurcation. In the fifth region (Figure 2.7(e)), the Hopf bifurcation becomes subcritical and a fold bifurcation of periodic orbits (FPO) emerges. In the last region (Figure 2.7(f)), the fold bifurcation of periodic orbits disappears, resulting in a bifurcation diagram with a subcritical Hopf bifurcation and no stable periodic orbits.

Region	**Range of the parameter s**	**Example**
Region 1	$s \in (-1.5, -1)$	Figure 2.7(a)
Region 2	$s \in (-1.567, -1.5)$	Figure 2.7(b)
Region 3	$s \in (-1.6, -1.567)$	Figure 2.7(c)
Region 4	$s \in (-1.75, -1.6)$	Figure 2.7(d)
Region 5	$s \in (-2.37, -1.75)$	Figure 2.7(e)
Region 6	$s \in (-\infty, -2.37)$	Figure 2.7(f)

Table 2.1: Qualitatively different s-dependent regions of the fast subsystem (2.2).

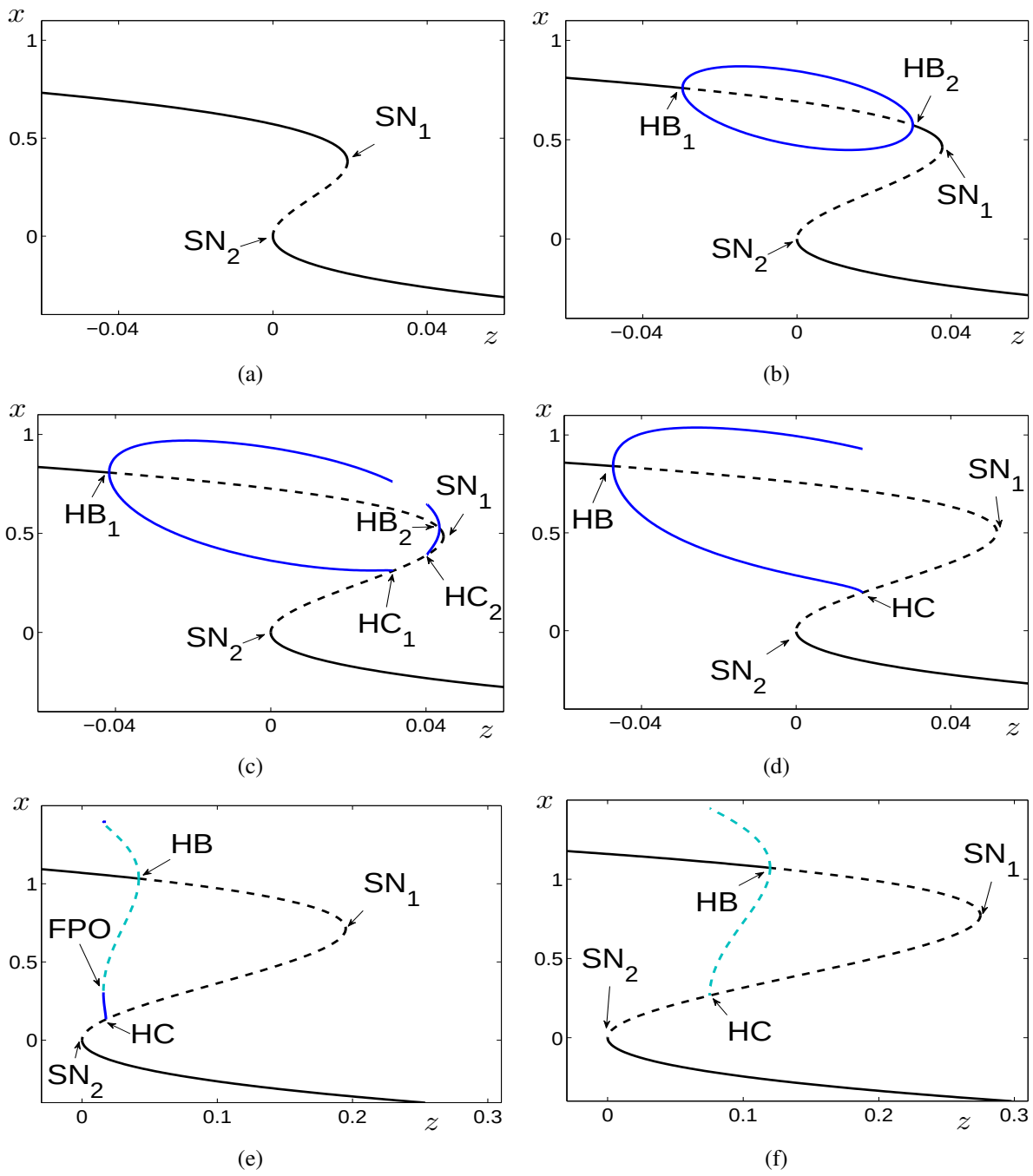

Figure 2.7: Representative bifurcation diagrams of the fast subsystem (2.2), for each region in Table 2.1. Regions from 1 to 6 are represented by panels (a) for $s = -1.4$, (b) for $s = -1.53$, (c) for $s = -1.57$, (d) for $s = -1.61$, (e) for $s = -2.15$, and (f) for $s = -2.38$, respectively. Values of other parameters are as for Figure 2.2. Line styles and labels are as for Figure 2.1. FPO−fold bifurcation of periodic orbits.

2.3 Analysis of the full system

This section focusses on the dynamics and the bursting behaviour in the full polynomial model, system (2.1), for sufficiently small ϵ. Our main goal is to find a direct transition from square-wave to pseudo-plateau bursting by changing only the parameter s and keeping all other parameters fixed. We also use this transition to associate each type of bursting with the corresponding s-dependent regions of the fast subsystem (see Table 2.1 and Figure 2.7).

We start with choosing values for a_1 and b_1 such that there is only one equilibrium of the full system, at least in the s-dependent regions where we expect bursting behaviour. We also wish to choose a_1 and b_1 to make the z-nullcline intersect with the curve of steady states of the fast subsystem at a saddle point very close to the homoclinic bifurcation of the fast subsystem, in order to produce ideal square-wave and pseudo-plateau bursting patterns [24, 32]. In general, the z-nullcline is a two-dimensional surface in the (x, y, z)-space. However, in our model, the equation of this surface does not depend on y, which means that we can represent the z-nullcline as a one-dimensional object in the (z, x)-plane. The z-nullcline is given by the linear equation:

$$x = \frac{k}{sa_1} z - \frac{b_1}{sa_1}. \tag{2.10}$$

Hence, the location and the slope of the z-nullcline both change as we vary s. We choose $a_1 = -0.1$ and $b_1 = -0.0279$. The choice ensures that the equilibrium point of the full system lies very close to the homoclinic bifurcation of the fast subsystem for two representative values of s, namely, $s = -1.61$ and $s = -2.15$.

Figure 2.8 shows the location of the z-nullcline superimposed on the bifurcation diagram of the fast subsystem, for (a) $s = -1.61$ and (b) $s = -2.15$. The equilibrium point of the full system corresponds to the intersection between the z-nullcline and the curve of steady states of the fast subsystem. Observe how equilibrium point of the full system is very close to saddle point involved in the homoclinic bifurcation (HC) of the fast subsystem in both panels. Note that the Hopf bifurcation (HB) of the fast subsystem is supercritical for $s = -1.61$, and subcritical for -2.15.

Square-wave bursting is typically associated with a supercritical Hopf bifurcation of the

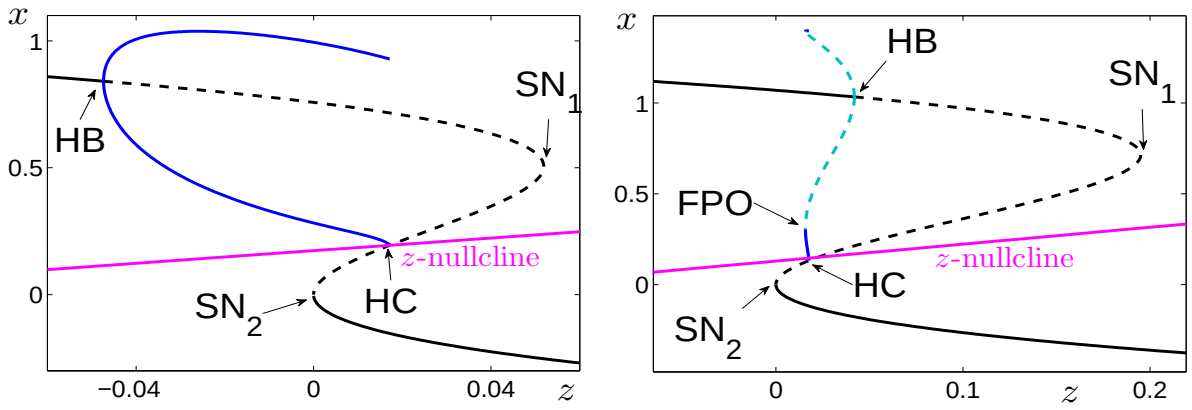

Figure 2.8: The z-nullcline (magenta) of system (2.1), for the choice $(a_1, b_1) = (-0.1, -0.0279)$, superimposed on the corresponding bifurcation diagrams of the fast subsystem, for (a) $s = -1.61$ and (b) $s = -2.15$. Here $a = 0.5$, $b = 1$, $\phi = 1$, $k = 0.2$. The black curve represents steady-state solutions of the fast subsystem; solid when stable, dashed when unstable. Blue curves indicate the maximum and minimum x-values of the periodic orbits; solid dark-blue when stable, dashed light-blue when unstable. HB−Hopf bifurcation; SN−saddle-node bifurcation; HC−homoclinic bifurcation; FPO−fold bifurcation of periodic orbits.

fast subsystem, whereas pseudo-plateau bursting is typically associated with a subcritical Hopf bifurcation of the fast subsystem [24, 32]. Therefore, we expect square-wave and pseudo-plateau bursting patterns to occur for $s = -1.61$ and $s = -2.15$, respectively. Figure 2.9 shows the bursting patterns observed at those values of s. Figure 2.9(a) shows two typical square-wave bursts for $s = -1.61$ and two different choices of ϵ, specifically, $\epsilon = 0.005$ and $\epsilon = 0.001$; the corresponding time series of x are shown in panels (c) and (e), respectively. By comparing the time series with the representation overlaid on the bifurcation diagram in panel (a), we can see that both bursts start on the lower branch of attracting steady states of the fast subsystem, which is the silent phase of the burst. The trajectories of both bursts jump up near the lower saddle-node bifurcation of the fast subsystem (SN_2) and start to follow the branch of the attracting periodic orbits of the fast subsystem; this is the active phase of the burst. Near the homoclinic bifurcation of the fast subsystem (HC), the trajectories drop back down to the lower branch of attracting steady states, after which the bursting orbit repeats. The main difference between the

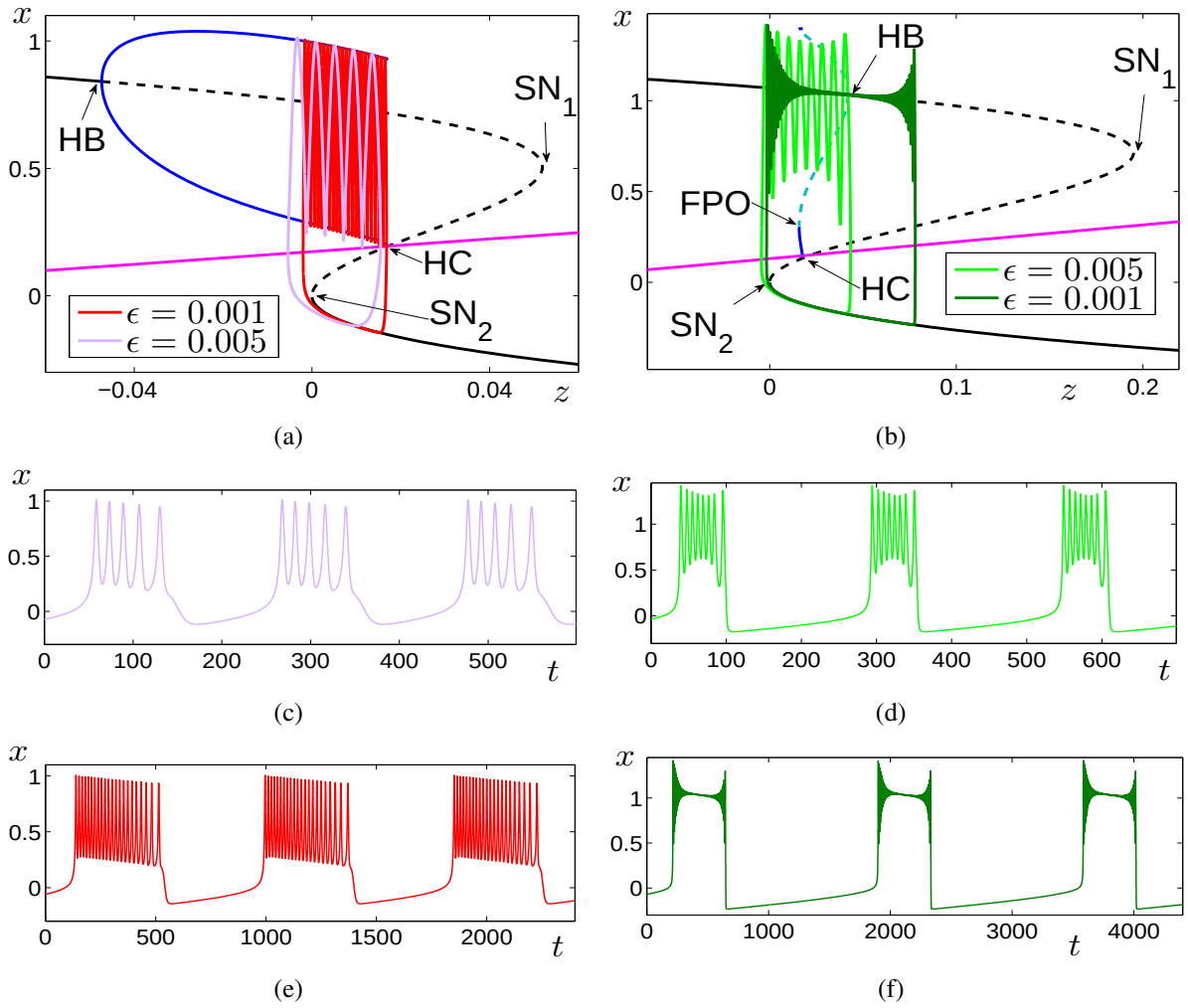

Figure 2.9: Bursting patterns in the full system (2.1), for two choices of s and two choices of ϵ. Panels (a) and (b) show square-wave ($s = -1.61$) and pseudo-plateau ($s = -2.15$) bursting patterns, respectively, overlaid on the corresponding bifurcation diagrams of the fast subsystem. Values of other parameters are as for Figure 2.8. Line styles and labels are as for Figure 2.8. Time series of the x-coordinate corresponding to the bursting solutions shown in panels (a) and (b) are shown in panels (c) and (d) for $\epsilon = 0.005$, respectively, and in panels (e) and (f) for $\epsilon = 0.001$, respectively.

two bursts is the number of spikes in the active phase.

Figure 2.9(b) shows two typical pseudo-plateau bursts for $s = -2.15$ and the same two

different choices of ϵ. The time series of x for $\epsilon = 0.005$ is shown in panel (d), and that for $\epsilon = 0.001$ in panel (f). As before, each trajectory starts on the lower branch of attracting steady states of the fast subsystem, then jumps up near the lower saddle-node bifurcation of the fast subsystem (SN_2) giving rise to the first spike. A number of spikes follow. The amplitudes of the spikes decrease at first as the trajectory is attracted to the upper branch of attracting steady states with complex eigenvalues (spiral sinks), then increase as the bursting orbit passes near a repellor. A repellor can be either a branch of repelling periodic orbits as in the case for $\epsilon = 0.005$ (the light green burst), or a branch of repelling steady states as in the case for $\epsilon = 0.001$ (the dark green burst). Eventually, when the spike amplitude is large enough, the trajectory drops back down to the lower branch of steady states.

We are interested in the mechanism by which square-wave bursting transforms into pseudo-plateau bursting. Figure 2.10 shows the bifurcation diagram of the full system for the case $\epsilon = 0.01$ with s varying in the range $[-2.27, -1.14]$, where there is only one equilibrium point. For $s = -1.14$, the equilibrium point is stable and it is the only attractor of the system. The equilibrium point changes stability through a supercritical Hopf bifurcation of the full system (H) at $s \approx -1.215$. As s decreases, different periodic solutions, characterised by different numbers of spikes within one overall period, are observed. The spike-adding transitions between branches of periodic orbits typically occur via saddle-node bifurcations of periodic orbits (SNPs) or period-doubling bifurcations (PDs). Nevertheless, the first four spike-adding transitions, approximately for the range $s \in (-1.531, -1.215)$, do not occur through any bifurcations, but rather arise as a continuous deformation between periodic orbits that exhibit different number of spikes. Note that we refer to the fold bifurcations of periodic orbits in the full system as saddle-node bifurcations of periodic orbits (SNPs) to distinguish them from those of the fast subsystem.

The square-wave regime in Figure 2.10 is represented by the red branch, given approximately by the range $s \in (-1.63, -1.567)$, and the pseudo-plateau regime is represented by the green branches, given roughly by the range $s \in (-2.27, -2.13)$. Blue branches represent periodic orbits of other types of behaviour. Note that square-wave bursting does not occur for s-values corresponding to regions 1 and 2 of Table 2.1, namely, for $-1.567 < s < -1$. The reason for that will be discussed in the next chapter.

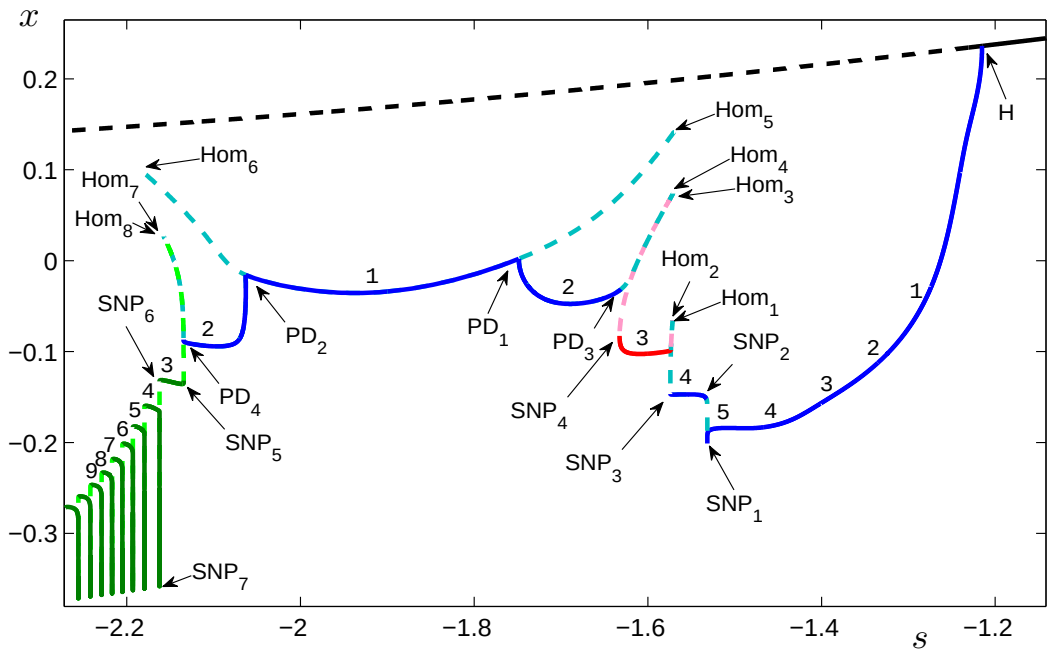

Figure 2.10: Bifurcation diagram of the full system (2.1), with s varying and $\epsilon = 0.01$. Values of other parameters are as for Figure 2.8. The black curve denotes the position of the equilibrium points, solid for stable and dashed for unstable. Coloured curves indicate the minimum x-values of the periodic orbits; solid and dark when stable, dashed and light when unstable. Various colours represent different bursting patterns: red for square-wave bursting; green for pseudo-plateau bursting; grey for the transitional bursting pattern (none in this case); blue for other types of behaviour. The numbers represent the number of spikes of the corresponding stable periodic orbits. H−Hopf bifurcation; SNP−saddle-node bifurcation of periodic orbits; PD−period doubling bifurcation; Hom−homoclinic bifurcation.

The 1-spike branch in the middle of Figure 2.10 goes through a period-doubling bifurcation at both ends (PD_1, PD_2) giving rise to a 2-spike branch on each side. Each 2-spike branch goes through another period-doubling bifurcation (PD_3, PD_4) giving rise to a 4-spike branch (not shown). This process of doubling the number of spikes via a cascade of period-doubling bifurcations has also been found in [19, 24, 32, 35]. The 1-spike periodic orbits do not exhibit any bursting behaviour. The 2-spike periodic orbits and all further period-doubled orbits are not considered to be square-wave or pseudo-plateau bursting because the trajectories for these orbits do not follow the lower branch of attracting steady states of the fast subsystem, that is,

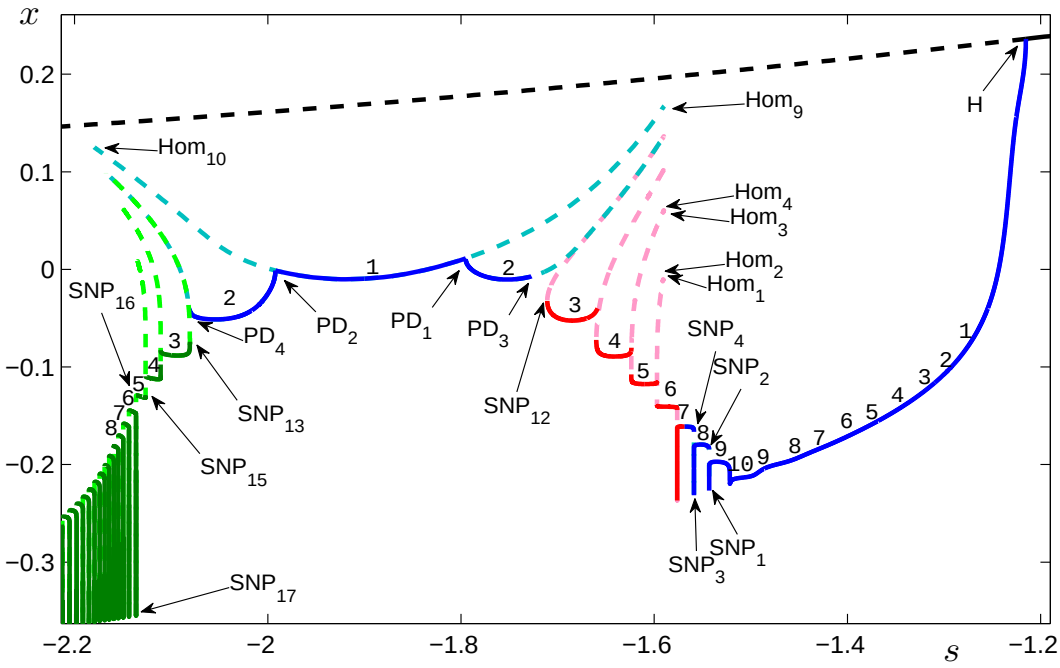

Figure 2.11: Bifurcation diagram of the full system (2.1), with s varying, $\epsilon = 0.005$. Values of other parameters are as for Figure 2.8. Line styles and labels are as for Figure 2.10.

they do not have a silent phase.

We are mainly interested in the transition between square-wave and pseudo-plateau bursting. As shown in Figure 2.10, the blue branches separate the square-wave and pseudo-plateau regimes. Therefore, there is no direct transition between the two bursting patterns for $\epsilon = 0.01$.

As we decrease ϵ, the structure of the bifurcation diagram stays qualitatively the same but with more spike-adding transitions within the same range of s. The 1-spike and 2-spike branches in the middle persist for smaller values of ϵ. Figure 2.11 shows the bifurcation diagram of the full system for $\epsilon = 0.005$. Observe that the square-wave regime seems to have become larger, but the pseudo-plateau regime remains fairly constant compared with Figure 2.10.

Further reduction of ϵ slows the computations down enormously, to the point where it is impractical to compute the whole bifurcation diagram. Therefore, we focus only on the left-hand side of the middle blue branches, where the system can exhibit both square-wave

and pseudo-plateau bursting for sufficiently small ϵ. In particular, we focus on the range $s \in [-2.100, -2.046]$, where we can see a transition between square-wave and pseudo-plateau bursting for $\epsilon = 0.001$. Figure 2.12(a) shows the bifurcation diagram of the full system for that range of s-values and $\epsilon = 0.001$. The regimes of square-wave (red) and pseudo-plateau (green) bursting occur approximately for $s \in [-2.072, -2.046]$ and $s \in [-2.100, -2.094]$, respectively. The grey curves between the square-wave and pseudo-plateau regimes correspond to transitional bursting patterns that are of neither square-wave nor pseudo-plateau type. Nonetheless, transitional bursting patterns exhibit properties of both square-wave and pseudo-plateau bursting.

Figure 2.12(a) shows that the transition occurs via spike-adding isolas. An isola is an isolated branch of periodic orbits which is typically formed by two branches, each terminates at a saddle-node bifurcation of periodic orbits (SNP) on both sides [24, 32]; here, all isolas terminate at homoclinic bifurcations. Note that an isola corresponding to bursts with n spikes lies next to an isola of bursts with $(n+1)$ spikes. This spike-adding mechanism has also been found in [24, 32]. In Figure 2.12(a), it appears that the different isolas are connected. However, these isolas are actually disjoint and the unstable parts of the branches just overlap. In particular, branches of periodic orbits for the square-wave and pseudo-plateau regimes are disjoint, that is, these branches do not belong to the same family of periodic orbits.

Figure 2.12(b) shows the bursting orbit for $s = -2.05$ which is an s-value representative of the square-wave regime coloured red in Figure 2.12(a). Observe how all of the spikes follow the branch of attracting periodic orbits of the fast subsystem. Note that square-wave bursting occurs despite the absence of a supercritical Hopf bifurcation in the underlying fast subsystem. Rather, the attracting periodic orbits of the fast subsystem are generated by a fold bifurcation of periodic orbits (FPO).

Figure 2.12(c) shows the bursting orbit for $s = -2.10$ which is an s-value representative of the pseudo-plateau regime coloured green in Figure 2.12(a). In this pseudo-plateau bursting, the amplitudes of the spikes initially decrease as the trajectory is attracted to the upper branch of spiral sinks of the fast subsystem, then increase as the trajectory gets repelled by the branch of repelling periodic orbits. None of the spikes follow the branch of attracting periodic orbits of the fast subsystem.

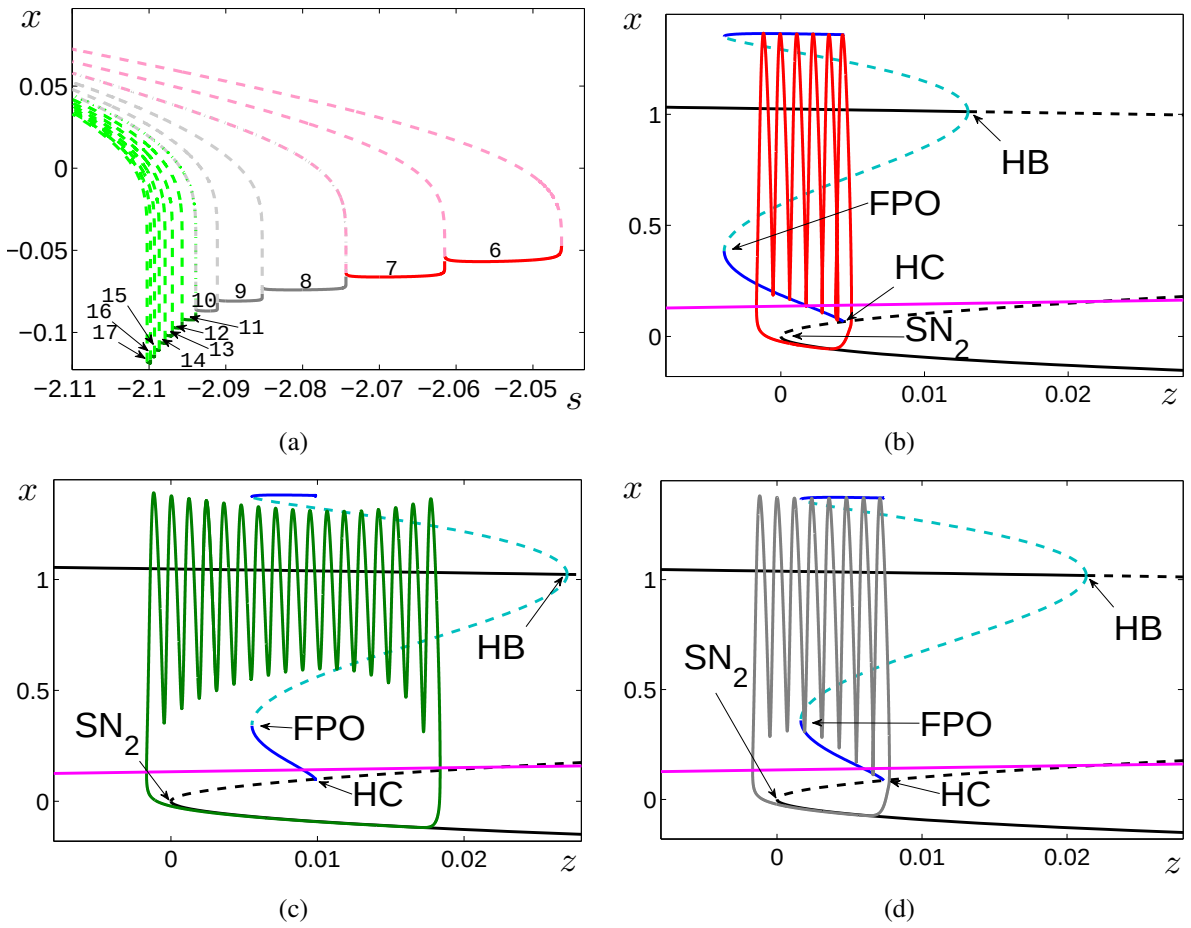

Figure 2.12: The transition between square-wave and pseudo-plateau bursting in the full system (2.1). Here, s is varying, $\epsilon = 0.001$, and values of other parameters are as for Figure 2.8. Panel (a) shows a partial bifurcation diagram of the full system with $s \in [-2.11, -2.046]$; line styles and labels are as for Figure 2.10. Panels (b), (c) and (d) show the bursting patterns in the full system overlaid on the corresponding bifurcation diagrams of the fast subsystem for the representative choices of $s = -2.05$, in the square-wave regime; $s = -2.10$, in the pseudo-plateau regime; $s = -2.08$, in the transitional bursting pattern regime, respectively. Line styles and labels for panels (b)-(d) are as for Figure 2.8.

Figure 2.12(d) shows the bursting orbit for $s = -2.08$ which is an s-value representative of the transitional bursting pattern regime coloured grey in Figure 2.12(a). In this transitional bursting pattern, some of the spikes follow the branch of attracting periodic orbits of the fast subsystem, and some of them do not. Note that for all three bursting patterns, the trajectory

overshoots the lower saddle-node bifurcation (SN_2) of the fast subsystem before jumping up.

We can see from Figure 2.12(b)-(d) that the main distinguisher between square-wave and pseudo-plateau bursting patterns is that the spikes follow the attracting periodic orbits in the fast subsystem for the case of square-wave bursting, and do not follow any branch of attracting periodic orbits for the case of pseudo-plateau bursting. In the transitional bursting pattern, some of the spikes follow the branch of attracting periodic orbits and some of them do not. While attracting periodic orbits of the fast subsystem exist for all three cases, only for the case of square-wave bursting, there exists a branch of attracting periodic orbits at the moment when the trajectory jumps up from the lower saddle-node bifurcation.

To sum up, we found a transition between square-wave and pseudo-plateau bursting for $\epsilon = 0.001$. However, the branches of periodic orbits for square-wave and pseudo-plateau bursting are isolated. Furthermore, we observed an overshoot of the trajectory near the lower saddle-node bifurcation of the fast subsystem before jumping up. In the next chapter, we propose defining criteria and conditions for square-wave, pseudo-plateau and transitional bursting patterns. We will use these criteria and conditions to motivate changes of parameters, so that a cleaner transition between the two bursting patterns can be observed.

Chapter 3

Characterisation of the different bursting patterns

There are many different bursting patterns and it is not always easy to decide which type a particular time series exhibits. In fact, biologists are sometimes ambivalent, which partly explains why the pseudo-plateau bursting pattern was discovered only recently [27]. Also, there are no clear mathematical definitions of different bursting patterns, at least not when considering the transition between square-wave and pseudo-plateau bursting.

In this chapter we propose characterising criteria and conditions that we use to distinguish between square-wave and pseudo-plateau bursting patterns. Here, we only consider systems with two fast variables and one slow variable. In particular, we consider systems in the form of system (1.1) with ϵ sufficiently small. Assuming that the functions f, g and h in system (1.1) are of the same order, we consider ϵ as the ratio between slow and fast timescales. In particular, we refer to x and y as fast variables, and z as the slow variable. Without loss of generality, we characterise the type of bursting with respect to the time series of x.

We set the criteria and conditions with the restriction that a classification of either square-wave or pseudo-plateau bursting should not change if the perturbation parameter ϵ is reduced. Therefore, we only classify bursting patterns for which ϵ is small enough, and regard those with larger ϵ-values as undecided cases. Some of these undecided cases are typically observed in the transition from square-wave to pseudo-plateau bursting and we discuss their properties in more

detail in Section 3.3.

The requirement that ϵ can be reduced without changing the bursting type implies that the classification is primarily defined by the bifurcation diagram of the fast subsystem, which we use as the main ingredient in our definitions. We also impose precise conditions to ensure the type of bursting is observed and discuss special cases.

3.1 Square-wave bursting

Generally, square-wave bursting exhibits relatively large spikes and the spike amplitudes are approximately even in size during the active phase (see Figure 1.1(a)). Loosely speaking, the spikes seem to be bounded by two straight near-horizontal lines represented by the maximum and minimum amplitudes of the attracting periodic orbits of the fast subsystem. As $\epsilon \to 0$, square-wave bursting generates more spikes, but the spiking envelope does not lose its shape.

Figure 3.1 shows the simplest form of square-wave bursting. Here, we use the generic polynomial model, system (2.1), with parameters $s = -1.61$, $\epsilon = 0.0005$, $a = 0.5$, $b = 1$, $\phi = 1$, $a_1 = -0.3$, $b_1 = -0.02$, and $k = 0.2$. We show the bursting orbit (red) overlaid on the underlying bifurcation diagram of the fast subsystem in the (z, x)-plane. Observe from the underlying bifurcation diagram of the fast subsystem that there are three co-existing branches of steady-state solutions indicated by the black curves; solid when stable and dashed when unstable. The interval of co-existence starts from a saddle-node bifurcation of the fast subsystem ($\mathsf{SN_2}$) for $z = 0$ and continues past $z = 0.018$. The two solid dark-blue curves indicate the maximum and minimum x-values of a branch of attracting periodic orbits. The branch of attracting periodic orbits exists already for $z < 0$, and ends at a homoclinic bifurcation (HC) for $z \approx 0.017$. Note also that the magenta-coloured z-nullcline intersects the steady-state branches only at one point, specifically, on the saddle branch of steady states very close to $\mathsf{SN_2}$. Starting from the lower branch of attracting steady states, the trajectory of the burst decreases in the z-direction and jumps up at $\mathsf{SN_2}$. In the active phase starts, the trajectory moves in the positive direction of the slow variable z. All spikes in the burst have a maximum and minimum in x that follow the maxima and minima of the attracting periodic orbits of the fast subsystem. Very close to HC, the trajectory drops back down to the lower branch of steady states after which the bursting

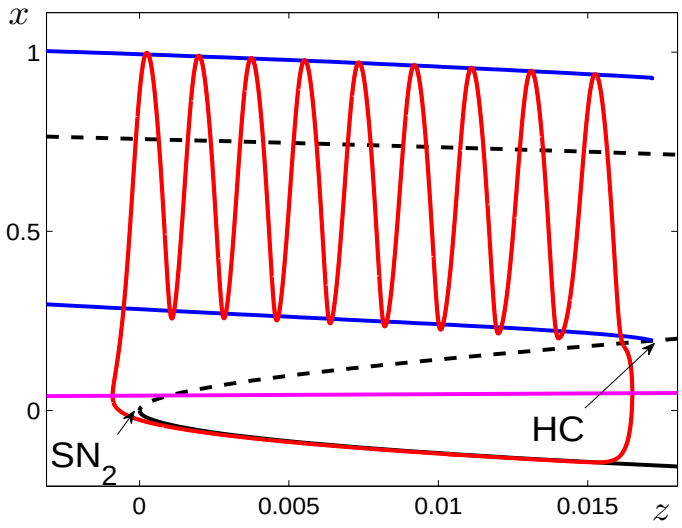

Figure 3.1: Square-wave bursting in system (2.1), overlaid on the corresponding bifurcation diagram of the fast subsystem. Here $s = -1.61$, $\epsilon = 0.0005$, $a = 0.5$, $b = 1$, $\phi = 1$, $a_1 = -0.3$, $b_1 = -0.02$, and $k = 0.2$. Line styles and labels are as for Figure 2.8.

orbit repeats.

Criteria for square-wave bursting

There are certain defining criteria that need to be met for the bursting to be called square wave. We use the example of square-wave bursting in Figure 3.1 as a guide to describe these criteria. Without loss of generality, starting on a lower branch of attracting steady states of the fast subsystem, a square-wave bursting trajectory should jump up at a saddle-node bifurcation, after which it starts the active phase. All spikes of the active phase follow a branch of attracting periodic orbits of the fast subsystem. The burst must exhibit at least two spikes, and the spike amplitudes should be relatively large and roughly even in size. Approximately at the end of the branch of attracting periodic orbits, the active phase ends and the trajectory drops back down to the lower branch of attracting steady states after which the bursting orbit repeats.

Based on these criteria, we generate sufficient conditions on the fast subsystem, the z-nullcline, and the timescale ratio (ϵ), that guarantee an appearance of a square-wave burst.

Conditions on the fast subsystem

In order to ensure that square-wave bursting occurs for sufficiently small fixed ϵ, the bifurcation diagram of the fast subsystem should satisfy the following conditions. The first condition states that there must be three co-existing steady-state solutions in the fast subsystem for an interval of values of the slow variable z. We denote this co-existence interval by Z_3. We require that one of the three branches of steady-state solutions is stable over the entire co-existence interval Z_3 and ends at a saddle-node bifurcation for $z = z_{SN}$, where it collides with a saddle branch of steady states. We call this stable branch the lower branch and the saddle branch the middle branch, and we assume that the saddle-node bifurcation occurs on the left-hand end of those two branches. Therefore, Z_3 is bounded from the left by the saddle-node bifurcation, namely by $z = z_{SN}$. We regard this lower branch of attracting steady states as the main attractor of the silent phase of the burst, and regard the saddle-node bifurcation as the end point of the silent phase and the starting point of the active phase.

The second condition states that there needs to be a branch of attracting periodic orbits surrounding the third (upper) branch of steady-state solutions. The amplitudes of the attracting periodic orbits should be relatively large and roughly even in size. This branch of attracting periodic orbits is regarded as the main attractor in the active phase for square-wave bursting; hence, it should not be surrounded by any other branch of periodic orbits. Without loss of generality, in the projection onto the (z, x)-plane, the maximum and the minimum of the attracting periodic orbits in Z_3 should lie above both the lower and middle branches of steady states. This branch of attracting periodic orbits should exist over an interval of z-values that includes $z = z_{SN}$, and terminate at some $z = z_{PO} > z_{SN}$, where $z_{PO} \in Z_3$. The termination must be such that the branch of attracting periodic orbits sustains its large amplitude, i.e., the termination should not be by a Hopf bifurcation. Depending on the choice of ϵ, the interval $z \in (z_{SN}, z_{PO})$ should be sufficiently large.

An example that satisfies all of these conditions is illustrated in Figure 3.1. Here, $z_{SN} = 0$ is the lower saddle-node bifurcation ($\mathsf{SN_2}$) and $z_{PO} \simeq 0.017$ is a homoclinic bifurcation (HC). The co-existence interval Z_3 is bounded from the left by $z_{SN} = 0$ and extends past $z = 0.018 > z_{PO}$.

Conditions on the nullcline of the slow variable

The location of the nullcline of the slow variable (the z-nullcline) in the full system is the second key ingredient that controls the appearance of square-wave bursting. Recall that, generally, the z-nullcline is a two-dimensional surface in the (x, y, z)-space. However, we can represent the z-nullcline as a one-dimensional object in the (z, x)-plane as illustrated in Figure 3.1. For square-wave bursting, the z-nullcline surface must intersect the steady-state solutions of the fast subsystem at one point on the middle branch, close to the saddle-node bifurcation at $z = z_{SN}$. Moreover, it should not intersect the steady-state solutions at any other point. As a result, there should be only one equilibrium point of the full system, and it should be unstable and close to the saddle-node bifurcation of the fast subsystem. The z-nullcline should be placed such that the slow variable z is decreasing for the region in which the lower branch of steady states exists, and increasing on the other side of the nullcline. Ideally, the z-nullcline does not intersect the branch of attracting periodic orbits; the reason is discussed below. Note that all these conditions are satisfied for the example shown in Figure 3.1.

Conditions on the timescale ratio

We outlined conditions on the fast subsystem as well as the z-nullcline to ensure an appearance of square-wave bursting based on the assumption that the timescale ratio parameter ϵ is small enough. Here, we discuss what this means for our choice of ϵ. Essentially, we need the interval $z \in (z_{SN}, z_{PO})$ to be sufficiently large such that the bursting exhibits more than one spike. Therefore, if the difference $z_{PO} - z_{SN}$ is relatively small, then we need ϵ to be correspondingly small. The location of the z-nullcline also matters. In the limit as $\epsilon \to 0$, if the z-nullcline intersects a branch of attracting periodic orbits, square-wave bursting could be lost and the system will exhibit tonic spiking without a silent phase [3]. However, we choose not to be very strict with this condition, because for fixed values of ϵ, we sometimes observe all features of square-wave bursting even if the z-nullcline intersects the branch of attracting periodic orbits; for example, see the case shown in Figure 2.12(b).

Special cases where square-wave bursting is found

Square-wave bursting has previously been associated with a supercritical Hopf bifurcation on the upper branch of steady states of the fast subsystem [24, 32], but we do not regard that as a condition. For instance, square-wave bursting could appear if the fast subsystem exhibits both a subcritical Hopf bifurcation and a fold bifurcation of periodic orbits. An example of such a case is illustrated in Figure 2.12(b); note that the fold bifurcation of periodic orbits lies to the left of the saddle-node bifurcation, that is, outside the co-existence interval Z_3. Hence, an attracting periodic orbit exists for $z = z_{SN}$.

Square-wave bursting has also been associated with a homoclinic bifurcation of the fast subsystem. In fact, square-wave bursting is often called fold/homoclinic bursting, which means that the burst initiates at a fold (saddle-node) bifurcation and terminates at a homoclinic bifurcation [13, 23, 24, 32]. Our characterisation includes cases where square-wave bursting does not terminate at a homoclinic bifurcation. In particular, we include the case where a burst initiates at a saddle-node bifurcation and terminates at a fold bifurcation of periodic orbits, as long as the criteria discussed above are met.

If the amplitudes of the attracting periodic orbits of the fast subsystem at the beginning of the z-interval during the active phase are much smaller than those at the end of that interval, then we expect the spikes of the burst to increase dramatically in amplitude; we do not classify this as a type of square-wave bursting. Similarly, if the branch of attracting periodic orbits terminates at a Hopf bifurcation, the corresponding spike amplitudes will decrease dramatically as we approach the end of the active phase; this type of bursting is also not classified as square-wave bursting.

3.2 Pseudo-plateau bursting

Generally, pseudo-plateau bursting exhibits relatively small spikes (see Figure 1.1(b)). Moreover, the spike amplitudes in pseudo-plateau bursting initially decrease and then increase again. Loosely speaking, the spikes seem to be bounded by two parabolic curves. As $\epsilon \to 0$, pseudo-plateau bursting develops more spikes, but the spike amplitudes virtually decrease to zero, ex-

cept for the first and last few spikes of the burst.

Figure 3.2 shows the simplest form of pseudo-plateau bursting. Here, we also use system (2.1), but with $s = -2.4$, $\epsilon = 0.007$, $a = 0.5$, $b = 1$, $\phi = 1$, $a_1 = -0.3$, $b_1 = -0.08$, and $k = 0.2$. The bursting orbit (green) is overlaid on the underlying bifurcation diagram of the fast subsystem in the (z, x)-plane. There are three co-existing branches of steady-state solutions of the fast subsystem that exist from $z = 0$ to past $z = 0.26$. The branches of steady-state solutions are denoted by the black curves; solid when stable and dashed when unstable. A saddle-node bifurcation ($\mathsf{SN_2}$), a homoclinic bifurcation (HC), and a subcritical Hopf bifurcation (HB) occur for $z = 0$, $z \approx 0.081$, and $z \approx 0.127$, respectively. Note that the upper branch of steady states is stable for $z \in (0, 0.127)$, and unstable for $z \in (0.127, 0.260)$. There is a branch of repelling periodic orbits (the dashed light-blue curves) emanating from HB. The figure also shows that the magenta-coloured z-nullcline intersects the steady-state solutions only at one point, specifically, on the middle branch very close to $\mathsf{SN_2}$. Starting from the lower branch of attracting steady states, the trajectory of the burst jumps up at $\mathsf{SN_2}$ to develop its first spike. The following spikes get attracted by a branch of attracting steady states with complex eigenvalues (spiral sinks) and decrease in amplitude. After passing the Hopf bifurcation (HB), the spikes increase in amplitude due to a branch of repelling steady states with complex eigenvalues (spiral sources). Eventually, the trajectory drops back down to the lower branch of steady states and the bursting orbit repeats.

Criteria for pseudo-plateau bursting

In order for the bursting to be called pseudo plateau, there are some defining criteria that need to be satisfied. We use the example of pseudo-plateau bursting in Figure 3.2 as a guide to describe these criteria. By following the pseudo-plateau burst from the lower branch of attracting steady states of the fast subsystem, the trajectory should jump up at the saddle-node bifurcation and then start the active phase. The spikes of the active phase get attracted to a branch of spiral sinks and, hence, decrease in amplitude. Once the trajectory encounters a repellor of the fast subsystem, the spikes increase in amplitude. This repellor can either be a branch of repelling steady states, as in Figure 3.2, or a branch of repelling periodic orbits, as in Figure 2.12(c). The

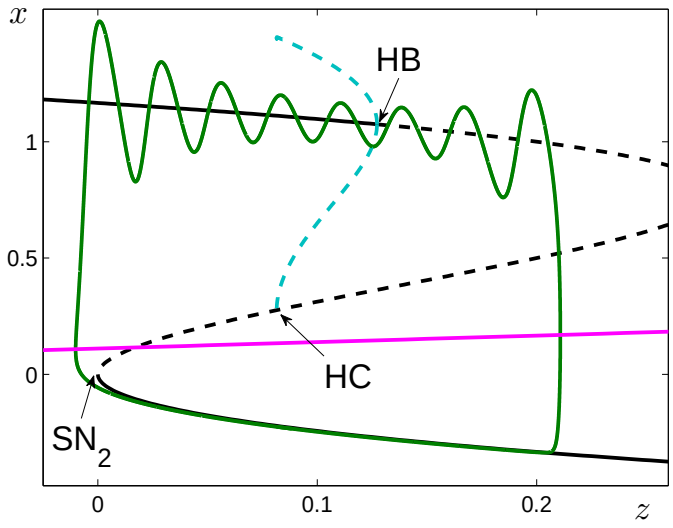

Figure 3.2: Pseudo-plateau bursting in system (2.1), overlaid on the corresponding bifurcation diagram of the fast subsystem. Here $s = -2.4$, $\epsilon = 0.007$, $a = 0.5$, $b = 1$, $\phi = 1$, $a_1 = -0.3$, $b_1 = -0.08$, and $k = 0.2$. Line styles and labels are as for Figure 2.8.

spikes must never follow a branch of attracting periodic orbits of the fast subsystem, if it ever exists. As illustrated in Figure 3.2, after a last large spike, the trajectory drops back down to the lower branch of attracting steady states to repeat the bursting orbit. The z-value at which the active phase ends is less well-defined than for square-wave bursting. The precise moment of the end of the active phase is organized by the stable manifold of the saddle branch of steady states of the fast subsystem, and by the choice of ϵ [22].

We use these criteria to outline sufficient conditions on the fast subsystem, the z-nullcline, and the timescale ratio (ϵ), that guarantee an occurrence of pseudo-plateau bursting.

Conditions on the fast subsystem

In order to assure the occurrence of pseudo-plateau bursting for sufficiently small ϵ, the following conditions on the bifurcation diagram of the fast subsystem should apply. First of all, as for square-wave bursting, there should be three co-existing solutions for $z \in Z_3$, where Z_3 is the co-existence interval. Like the case of square-wave bursting, one branch, namely, the

lower branch of steady states needs to be stable over the entire co-existence interval Z_3 and to collide with the middle saddle branch at a saddle-node bifurcation. Without loss of generality, we assume that the saddle-node bifurcation occurs for some $z = z_{SN}$ on the left-hand end of the lower and middle branches; hence, Z_3 is bounded from the left by $z = z_{SN}$. As before, we regard this lower branch of attracting steady states as the main attractor of the silent phase, and regard the saddle-node bifurcation as a critical point that separates the silent and active phases.

The second condition requires the existence of a Hopf bifurcation, usually subcritical, on the upper branch of steady-state solutions. This Hopf bifurcation should occur for $z = z_{HB} \in Z_3$ where $z_{HB} > z_{SN}$. If there is a branch of attracting periodic orbits, it should exist only over a relatively small interval of z, such that it does not attract the bursting trajectory. There must be no attracting periodic orbits of the fast subsystem existing for $z = z_{SN}$.

The third condition states that the upper branch of steady states must have complex eigenvalues with negative real parts (spiral sinks) for $z \in (z_{SN}, z_{HB})$. Moreover, the upper branch of steady states for $z > z_{HB}$ needs to be of type spiral source for a sufficient interval of $z \in Z_3$. More precisely, the upper branch of steady states should not be stable for the interval $z \in (z_{HB}, 2z_{HB} - z_{SN})$.

An example that satisfies all of these conditions is illustrated in Figure 3.2. Here, the saddle-node bifurcation occurs for $z_{SN} = 0$, and the Hopf bifurcation occurs for $z_{HB} \approx 0.127$. The upper branch of steady states consists of spiral sinks for $z \in (z_{SN}, z_{HB}) \approx (0, 0.127)$, and spiral sources at least for $z \in (z_{HB}, 2z_{HB} - z_{SN}) \approx (0.127, 0.254)$. Note that there are no periodic orbits of the fast subsystem existing for $z = z_{SN}$.

Conditions on the nullcline of the slow variable

As for square-wave bursting, the z-nullcline should intersect the steady-state solutions of the fast subsystem only at one point on the middle branch, close to the saddle-node bifurcation at $z = z_{SN}$. The z-nullcline should not intersect the steady-state solutions at any other point. Furthermore, the z-nullcline should be placed in the system such that $\dot{z} < 0$ in the region in which the lower branch of steady states exists, and $\dot{z} > 0$ on the other side of the nullcline. These conditions are satisfied for the example in Figure 3.2.

Conditions on the timescale ratio

The conditions for pseudo-plateau bursting on the fast subsystem and the z-nullcline are based on the assumption that ϵ is sufficiently small. In particular, the requirement that there are no periodic orbits of the fast subsystem existing for $z = z_{SN}$ implies that there are no periodic orbits for $z \in (z_{SN}, z_{SN} + \sigma)$, for some sufficiently small positive constant σ. Relatively speaking, the smaller σ is, the smaller ϵ needs to be in order for the bursting orbit to have enough time to get attracted to the upper branch of spiral sinks of the fast subsystem. In other words, the minimum value of the quantity σ required to observe pseudo-plateau bursting depends on the value of the timescale ratio parameter ϵ.

As mentioned earlier, the z-value at which the active phase ends depends on the timescale parameter ϵ. In particular, when ϵ is small enough, the active phase of pseudo-plateau bursting always ends after passing through the Hopf bifurcation of the fast subsystem. More precisely, for sufficiently small ϵ, the time spent towards the end of the active phase spiralling around the branch of repelling steady states will be the same as the time spent spiralling around the attracting steady states at the beginning of active phase. In other words, the active phase occurs roughly in the interval $z \in (z_{SN}, 2z_{HB} - z_{SN})$ with the Hopf bifurcation occurring exactly in the middle, provided the branch of spiral sources exists at least for $z \in (z_{HB}, 2z_{HB} - z_{SN})$. This phenomenon is called "persistence of stability loss" [20, 21], or "slow passage through a Hopf bifurcation" [1].

Special cases where pseudo-plateau bursting is found

Pseudo-plateau bursting has previously been associated with a subcritical Hopf bifurcation on the upper branch of the fast subsystem [23, 24, 32], but we do not consider the type of criticality of the Hopf bifurcation as a condition. For instance, pseudo-plateau bursting can occur if there is a supercritical Hopf bifurcation on the upper branch of steady states of the fast subsystem in Z_3, provided the branch of attracting periodic orbits exists only over a short range of z, such that it does not attract the bursting trajectory.

Pseudo-plateau bursting has also been given the name fold/subHopf bursting, that is, the burst starts at a fold bifurcation and ends at a subcritical Hopf bifurcation [23, 24, 32]. How-

ever, there are many cases of pseudo-plateau bursting where the active phase ends before or after reaching a Hopf bifurcation of the fast subsystem. For example, consider the burst in Figure 2.12(c) for which the active phase ends before reaching the Hopf bifurcation; or the burst in Figure 3.2 for which the active phase ends after passing through the Hopf bifurcation.

3.3 The transitional bursting patterns

The transition between square-wave and pseudo-plateau bursting could occur via various mechanisms and, hence, there are various corresponding types of transitional bursting patterns. However, only one of these mechanisms can be regarded as direct, meaning that the corresponding transitional bursting pattern disappears in the limit $\epsilon \to 0$, resulting in a direct transition between square-wave and pseudo-plateau bursting. We call this type of transitional bursting pattern the standard transitional bursting pattern and we discuss it in detail; we regard the other types as special cases.

The standard transitional bursting pattern exhibits characteristics of both square-wave and pseudo-plateau bursting. Figure 3.3 shows a typical form of the standard transitional bursting pattern. Here, we use system (2.1) with $s = -2.08$, $\epsilon = 0.0001$, $a = 0.5$, $b = 1$, $\phi = 1$, $a_1 = -0.3$, $b_1 = -0.02$, and $k = 0.2$. The figure shows that there are three co-existing steady-state solutions of the fast subsystem which are indicated by the black curves; solid when stable and dashed when unstable. The interval of co-existing solutions extends from $z = 0$, where there is a saddle-node bifurcation (SN_2), to past $z = 0.0087$. There are also two co-existing branches of periodic orbits indicated by the blue curves that mark the maximum and minimum x-coordinates. The solid dark-blue curves correspond to attracting periodic orbits, and the dashed light-blue curves correspond to repelling periodic orbits. These branches are bounded from the left by a fold bifurcation of periodic orbits (FPO) for $z \approx 0.0017$. The branch of attracting periodic orbits terminates at a homoclinic bifurcation (HC) for $z \approx 0.0074$. The figure also shows that the magenta-coloured z-nullcline intersects the the curve of steady states on the middle branch very close to SN_2. The bursting orbit is overlaid on this bifurcation diagram using different colours to indicate its characteristics. In the green part of the active phase, the burst behaves like pseudo-plateau bursting where the spikes do not follow any branch

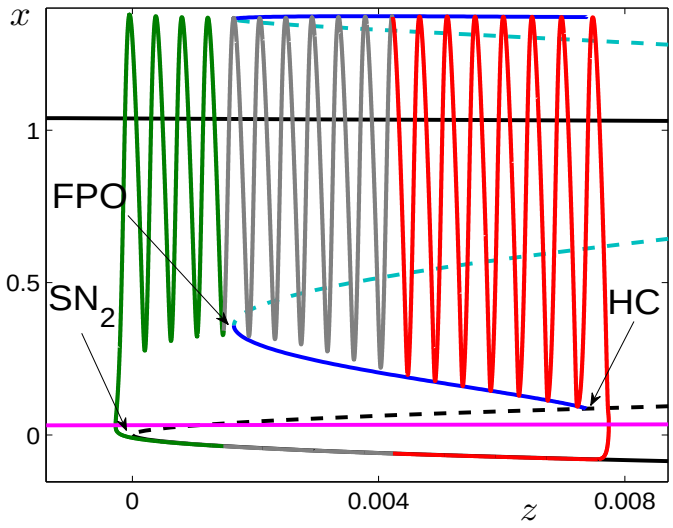

Figure 3.3: The standard transitional bursting pattern in system (2.1), overlaid on the corresponding bifurcation diagram of the fast subsystem. Here $s = -2.08$, $\epsilon = 0.0001$, $a = 0.5$, $b = 1$, $\phi = 1$, $a_1 = -0.3$, $b_1 = -0.02$, and $k = 0.2$. Line styles and labels are as for Figure 2.8. The green part of the burst behaves like pseudo-plateau bursting, the red part behaves like square-wave bursting, and the grey part behaves like neither. Note from the criteria for square-wave and pseudo-plateau bursting that this transitional bursting pattern cannot be classified as either of them.

of attracting periodic orbits. In the red part of the active phase, all spikes follow the attracting periodic orbits of the fast subsystem, and the burst behaves like square-wave bursting. The grey part of the active phase is an intermediate case, where the spikes follow the maxima in x of the attracting periodic orbits of the fast subsystem but not their minima. The bursting in Figure 3.3 cannot be classified as square-wave bursting, because there are no attracting periodic orbits for $z = z_{SN}$ and, hence, some of the spikes do not follow the branch of attracting periodic orbits. This bursting is also not of pseudo-plateau type because some of the spikes do follow the branch of attracting periodic orbits.

Criteria for the standard transitional bursting pattern

We propose defining criteria for the standard transitional bursting pattern using Figure 3.3 as a guide. As for the other bursting patterns, the active phase starts after the trajectory of a standard

transitional bursting pattern jumps up at a saddle-node bifurcation. Initially, the trajectory of the active phase spirals around a branch of spiral sinks and, hence, the spikes decrease in amplitude. Then the spikes start to follow a branch of attracting periodic orbits which means that the amplitude increases. As shown in Figure 3.3, some of the spikes behave like square-wave bursting and some of them behave like pseudo-plateau bursting, that is, some of the spikes follow a branch of attracting periodic orbits of the fast subsystem, and some of them do not. As for square-wave bursting, at the end of the branch of attracting periodic orbits, the trajectory drops back down to the lower branch of steady states after which the bursting orbit repeats.

Based on these criteria, we outline sufficient conditions on the fast subsystem, the z-nullcline and the timescale ratio ϵ, that guarantee appearance of a standard transitional bursting pattern. Unlike the cases of square-wave and pseudo-plateau bursting, the standard transitional bursting pattern vanishes in the limit as $\epsilon \to 0$. Therefore, our conditions for the standard transitional bursting pattern hold only for relatively large values of ϵ.

Conditions on the fast subsystem

In order to obtain a standard transitional bursting pattern, the bifurcation diagram of the fast subsystem should have a mix of properties from those for square-wave and pseudo-plateau bursting. In general, a direct transition mechanism requires the corresponding transitional bursting pattern to transform into either square-wave or pseudo-plateau bursting in the limit as $\epsilon \to 0$. In particular, the standard transitional bursting pattern that we describe, always transforms into pseudo-plateau bursting as $\epsilon \to 0$.

As before, we require three co-existing steady-state solutions for $z \in Z_3$ including a stable lower branch that collides with a middle saddle branch at a saddle-node bifurcation for $z = z_{SN}$ on the left-hand end of those two branches.

We also require a branch of attracting periodic orbits that starts at a fold bifurcation of periodic orbits for $z = z_{FPO} \in Z_3$ and ends for some $z = z_{PO} \in Z_3$, where $z_{SN} < z_{FPO} < z_{PO}$. However, there should be no branch of periodic orbits for $z = z_{SN}$. Without loss of generality, in the projection onto the (z, x)-plane, the maximum and the minimum of the attracting periodic orbits in Z_3 should lie above both the lower and middle branches of steady states. The ampli-

tudes of the attracting periodic orbits along this branch should be relatively large and roughly even in size.

Furthermore, we require the standard transitional bursting pattern to transform into pseudo-plateau bursting in the limit as $\epsilon \to 0$. Therefore, we need a Hopf bifurcation on the upper branch of steady states for $z = z_{HB} \in Z_3$, and we require the steady states on the upper branch to be spiral sinks for $z \in (z_{SN}, z_{HB})$, and spiral sources for a sufficiently large z-interval to the right of $z = z_{HB}$.

An example that satisfies all these conditions is illustrated in Figure 3.3. Note that the branch of periodic orbits starts at a fold bifurcation of periodic orbits (FPO) for $z_{FPO} \approx 0.0017 > z_{SN}$, and ends at a homoclinic bifurcation (HC) for $z_{PO} \approx 0.0074 > z_{FPO}$. The Hopf bifurcation required for the standard transitional bursting pattern is not shown, but occurs for $z_{HB} \approx 0.0213$. Moreover, the upper branch consists of spiral sinks for $z \in (z_{SN}, z_{HB}) \approx (0, 0.0213)$, and spiral sources at least for $z \in (z_{HB}, 2z_{HB} - z_{SN}) \approx (0.0213, 0.0426)$

Conditions on the nullcline of the slow variable

The conditions on the z-nullcline are the same as for pseudo-plateau bursting discussed in Section 3.2.

Conditions on the timescale ratio

Unlike square-wave and pseudo-plateau bursting, the standard transitional bursting pattern does not persist when ϵ is very small. Therefore, we require ϵ to be small enough for the trajectories to get attracted initially to the branch of spiral sinks, but large enough that eventually, the trajectory follows the branch of attracting periodic orbits. When ϵ is sufficiently reduced, the spikes of the standard transitional bursting pattern will cease to follow the branch of attracting periodic orbits because of the "persistence of stability loss" phenomenon [20, 21]. As a result, the standard transitional bursting pattern will transform into pseudo-plateau bursting when ϵ is sufficiently reduced.

Special cases of transitional bursting patterns

There are other types of transitional bursting patterns. These types appear in indirect transitions between square-wave and pseudo-plateau bursting, but they do not appear in our model.

One possible special type of transitional bursting pattern occurs when there is branch of attracting periodic orbits that emanates from a supercritical Hopf bifurcation on the upper branch of steady states for $z = z_{HB} \in Z_3$ and ends at some $z = z_{PO} \in Z_3$, where $z_{SN} < z_{HB} < z_{PO}$, while the steady states on the upper branch for $z \in (z_{SN}, z_{HB})$ are spiral sinks. By an appropriate change of parameters, this type of transitional bursting pattern can transform into either square-wave or pseudo-plateau bursting. For instance, if we move the Hopf bifurcation sufficiently to the left of the saddle-node bifurcation, the bursting pattern becomes square-wave bursting. On the other hand, if we allow the branch of attracting periodic orbits to exist over a relatively small z-interval, then the system exhibits pseudo-plateau bursting for sufficiently small ϵ. Unlike the standard transitional bursting pattern, this type of transitional bursting pattern can possibly persist in the limit as $\epsilon \to 0$, namely, when $z_{PO} > 2z_{HB} - z_{SN}$.

There are also other possible types of transitional bursting pattern which are more complicated; this is an interesting direction for future work and is beyond the scope of this thesis.

In summary, the main distinguisher between the three bursting patterns is that all of the spikes in square-wave bursting follow a branch of attracting periodic orbits of the fast subsystem, whereas none of the spikes in pseudo-plateau bursting do. Furthermore, we stipulate that we can only get square-wave bursting if there exists an attracting periodic orbit for $z = z_{SN}$. The transitional bursting patterns are considered as intermediate cases where some of the spikes follow the attracting periodic orbits, and some of them do not.

In the next chapter, we use the outlined criteria and conditions as a guide to make appropriate changes of parameter values for system (2.1), so that a direct transition between square-wave and pseudo-plateau bursting is obtained.

Chapter 4

Moving the nullcline of the slow variable

As we discussed in the previous chapter, the location of the z-nullcline relative to the bifurcation diagram of the underlying fast subsystem is important to ensure that square-wave bursting does not transform into tonic spiking in the limit as $\epsilon \to 0$ [3]. We decided to explore the effect of the location of the z-nullcline on the transition between square-wave and pseudo-plateau bursting. We can control the location of the z-nullcline in the generic polynomial model (2.1), by changing the parameters a_1 and b_1; see equation (2.10). In this chapter, we examine if a change in the location of the z-nullcline can result in a cleaner transition between the two bursting patterns.

In Chapter 2, the trajectories of the bursting patterns that we found for system (2.1) had an overshoot near the lower saddle-node bifurcation of the fast subsystem (see Figure 2.12(b)-(d)) before jumping up. We also found that the branches of periodic orbits for square-wave and pseudo-plateau bursting do not belong to the same family of periodic orbits of the full system (see Figure 2.12(a)). Here, we investigate whether a change in the location of the z-nullcline has any effect on those two issues. Therefore, we change the values of a_1 and b_1 from what they were in Chapter 2. In particular, we change b_1 from -0.0279 to -0.005, which places the equilibrium point of the full system, that is, the intersection point of the z-nullcline with the curve of steady-state solutions, closer to the lower saddle-node bifurcation of the fast subsystem (SN_2). In order to ensure that the location and the gradient of the z-nullcline do not change significantly when we vary s, we change a_1 from -0.1 to -0.3. This has the added benefit that

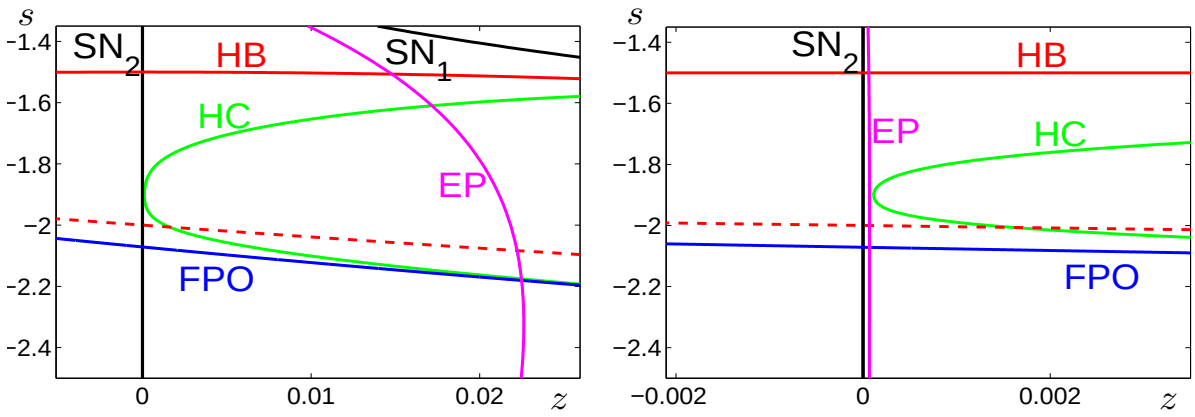

Figure 4.1: The locus of equilibrium points (EP, magenta) of the full system (2.1), in relation to the bifurcation curves of the fast subsystem in the (z, s)-plane. Panel (a) is for (a_1, b_1)=$(-0.1, -0.0279)$, as chosen in Chapter 2, and panel (b) is for the new choice (a_1, b_1)=$(-0.3, -0.005)$. Values of other parameters are as for Chapter 2: $a = 0.5$, $b = 1$, $\phi = 1$, $k = 0.2$. Line styles and labels are as for Figure 2.2.

the equilibrium point of the full system lies close to SN_2 over a wider range of s values. We also make sure with our new choice of parameters that the z-nullcline intersects the curve of steady states of the fast subsystem only once, specifically, on the middle branch of steady states. Therefore, the full system has a single unstable equilibrium point during the transition between square-wave and pseudo-plateau bursting.

Figure 4.1 illustrates the locus of equilibrium points (EP, magenta) of the full system in the (z, s)-plane relative to the loci of bifurcations of the fast subsystem. The black curves are curves of the saddle-node bifurcations. The curve of Hopf bifurcations (HB), the curve of homoclinic bifurcations (HC) and the curve of fold bifurcation of periodic orbits (FPO) are coloured red, green and blue, respectively. Figure 4.1(a) is for our initial choice of parameters (a_1, b_1)=$(-0.1, -0.0279)$, for which the equilibrium points of the full system are placed relatively far away from the lower saddle-node bifurcation of the fast subsystem (SN_2). Figure 4.1(b) shows that the new choice (a_1, b_1)=$(-0.3, -0.005)$ results in a much better placement of the equilibrium points, that is, the equilibrium points lie very close to SN_2 for a large range of s-values. Also, note that the equilibrium points for our new choice of a_1 and b_1 are

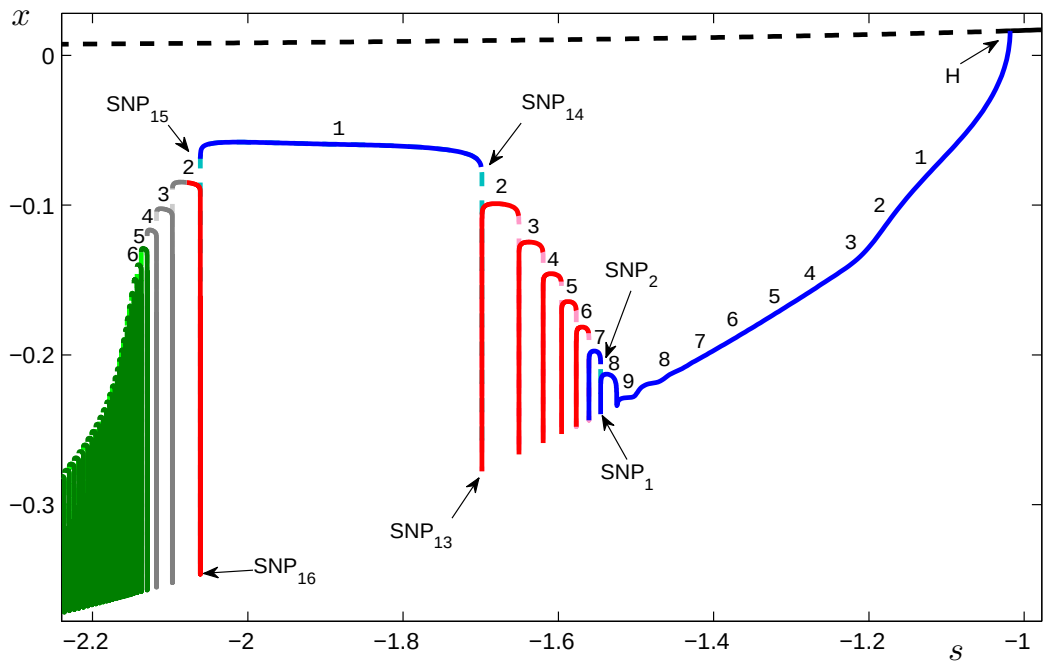

Figure 4.2: Bifurcation diagram of the full system (2.1) with s varying and $\epsilon = 0.001$. Here $a = 0.5$, $b = 1$, $\phi = 1$, and $k = 0.2$, and we set $a_1 = -0.3$, $b_1 = -0.005$. Line styles and labels are as for Figure 2.10.

located between the homoclinic bifurcations (HC) and the lower saddle-node bifurcations (SN_2) for this range in s.

We examine the effect of our new choice of parameters on the bursting patterns in the full system. Figure 4.2 shows the bifurcation diagram of the full system for (a_1, b_1)=$(-0.3,-0.005)$, with $\epsilon = 0.001$ and s varying. Notice that the family of periodic orbits of the full system is now fully connected, that is, there are no homoclinic bifurcations in the bifurcation diagram of the full system.

The square-wave regimes in Figure 4.2 are coloured red; they are approximately given by the intervals $s \in [-2.072, -2.06]$ and $s \in [-1.70, -1.567]$. There are two square-wave regimes because the periodic orbits for $s \in (-2.06, -1.70)$ exhibit only one spike without any bursting behaviour. Square-wave bursting does not occur for the range $s \in (-1.567, -1.5)$ which corresponds to the second s-dependent region of the fast subsystem in Table 2.1; a representative

example of a fast subsystem bifurcation structure for this range is illustrated in Figure 2.7(b). In this range, the active phase ends at a second Hopf bifurcation of the fast subsystem instead of a homoclinic bifurcation. As a result, the spike amplitudes decrease dramatically near the end of the active phase; as discussed in Section 3.1, we do not classify such bursting as square-wave bursting. Moreover, the system does not exhibit square-wave bursting for the range $s > -1.5$ because there are no periodic orbits of the fast subsystem in this range of s-values (see Figure 2.7(a)). The pseudo-plateau regime is coloured green and corresponds roughly to the range $s \in [-2.24, -2.13]$. The transitional bursting pattern regime is coloured grey and occurs approximately for $s \in (-2.13, -2.072)$. This regime is bounded from the right by $s \approx -2.072$ where the fold bifurcation of periodic orbits of the full system occurs for $z_{FP} \approx z_{SN} = 0$, hence, square-wave bursting is observed past that s-value, because an attracting periodic orbit of the fast subsystem exists for $z = z_{SN}$. Moreover, the transitional bursting pattern regime is bounded from the left by $s \approx -2.13$, where the branch of attracting periodic orbits of the fast subsystem exists over such a short z-interval that it no longer attracts the trajectory of the active phase. Hence, pseudo-plateau bursting is observed for $s < -2.13$.

As we decrease ϵ, the structure of the bifurcation diagram stays qualitatively the same but with more spike-adding transitions within the same range of s-values. In particular, for very small ϵ (e.g., $\epsilon = 0.00001$), we find that the 1-spike branch for $s \in (-2.06, -1.70)$ becomes a square-wave regime, and all square-wave regimes merge into a single connected family of periodic orbits (not shown).

Note that there is a direct transition between square-wave and pseudo-plateau bursting on the left-hand side of the 1-spike family of periodic orbits in Figure 4.2, but the square-wave regime is very small and only consists of a burst with two spikes. We make this regime larger by using a moderately smaller value of ϵ; specifically, we use $\epsilon = 0.0001$.

Figure 4.3 illustrates a direct transition between square-wave and pseudo-plateau bursting for the range $s \in [-2.09, -2.04]$ with $\epsilon = 0.0001$. Figure 4.3(a) shows that the transition occurs via a sequence of pairs of saddle-node bifurcations of periodic orbits (SNPs). This process of spike adding through pairs of SNPs was also reported in [19, 24, 32], and is called spike adding via a cascade of pairs of SNPs. Recall that we refer to fold bifurcations of periodic orbits in the full system as saddle-node bifurcations of periodic orbits (SNPs). Observe

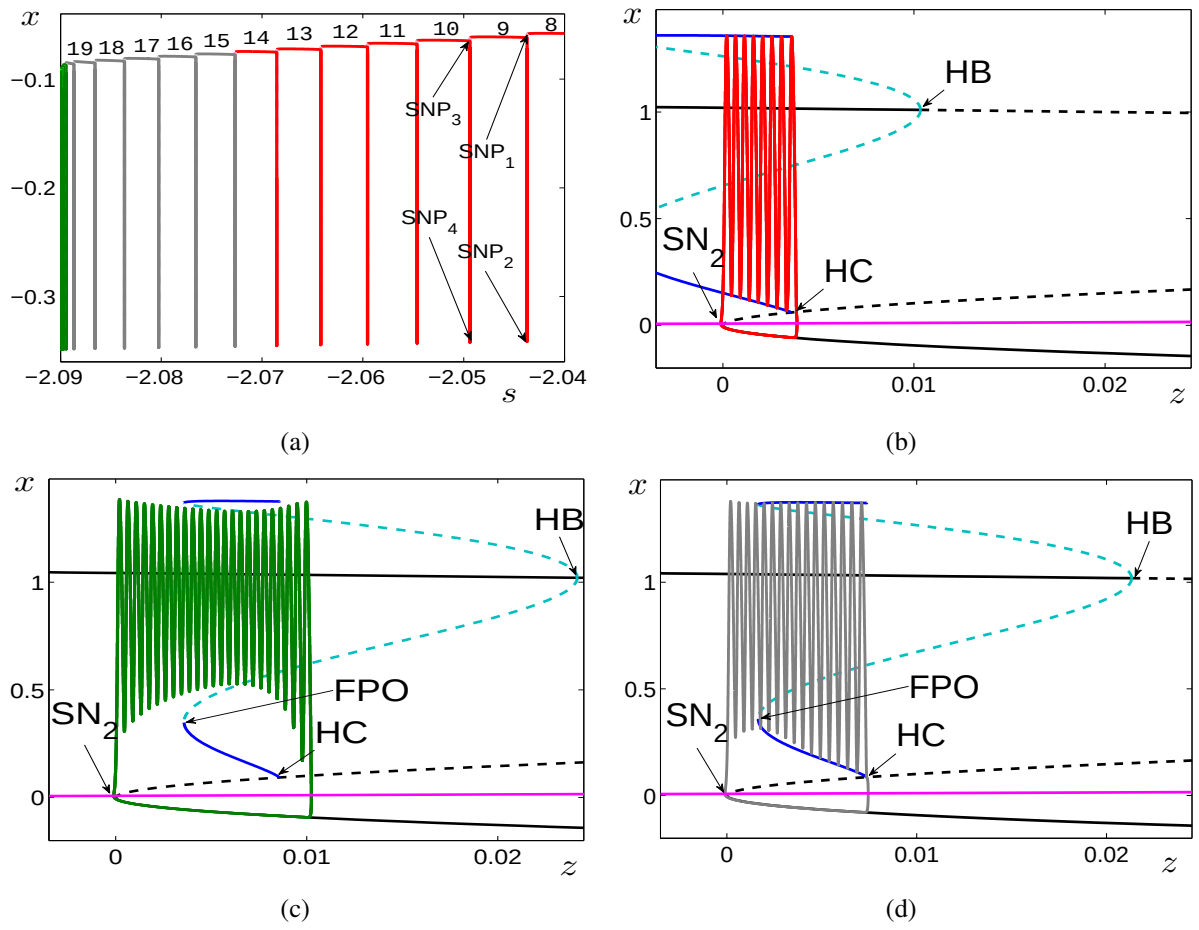

Figure 4.3: The transition between square-wave and pseudo-plateau bursting in the full system (2.1). Values of parameters are as for Figure 4.2, except that $\epsilon = 0.0001$. Panel (a) shows the bifurcation diagram of the full system with $s \in [-2.09, -2.04]$; line styles and labels are as for Figure 2.10. Panels (b), (c) and (d) show the bursting patterns in the full system overlaid on the corresponding bifurcation diagrams of the fast subsystem for the representative choices of $s = -2.04$, in the square-wave regime; $s = -2.09$, in the pseudo-plateau regime; and $s = -2.08$, in the transitional bursting pattern regime, respectively. Line styles and labels for panels (b)-(d) are as for Figure 2.8.

how the periodic orbits of square-wave bursting, pseudo-plateau bursting and the transitional bursting pattern are all connected through one single family. The bursting regimes are approximately defined by $s \in [-2.072, -2.04]$ for square-wave bursting (red), $s \in [-2.09 - 2.0894]$ for pseudo-plateau bursting (green), and $s \in (-2.0894, -2.072)$ for the standard transitional

bursting pattern (grey). These bounds are determined in the same way as for Figure 4.2. The transitional bursting pattern regime is bounded from the right by $s \approx -2.072$ where the fold bifurcation of periodic orbits of the full system occurs for $z_{FP} \approx z_{SN} = 0$. This regime is bounded from the left by $s \approx -2.0894$, where the branch of attracting periodic orbits of the fast subsystem exists over such a short z-interval such that it no longer attracts the trajectory of the active phase. Note that the transitional bursting pattern regime became smaller when we reduced ϵ from 0.001 to 0.0001. This is to be expected because the standard transitional bursting pattern transforms into pseudo-plateau bursting when ϵ is sufficiently reduced. In fact, in the limit as $\epsilon \to 0$, the whole transitional bursting pattern regime vanishes and the pseudo-plateau regime grows.

Panels (b)-(d) of Figure 4.3 show representative bursting patterns from the three different regimes overlaid on the corresponding bifurcation diagram of the fast subsystem. For all three panels the required co-existence interval Z_3 starts from the lower saddle-node bifurcation of the fast subsystem for $z_{SN} = 0$ and extends past $z = 0.024$; and the lower branch of steady states is stable. Also for all three cases, the z-nullcline intersects the middle branch of steady states very close to the lower saddle-node bifurcation of the fast subsystem ($\mathsf{SN_2}$); as a result, the trajectory does not overshoot $\mathsf{SN_2}$ before jumping up.

Figure 4.3(b) shows the square-wave bursting pattern for $s = -2.04$, which is representative for the square-wave regime in Figure 4.3(a). Note that the burst satisfies all the conditions and criteria of square-wave bursting that we outlined in Section 3.1. In the underlying fast subsystem, there is a branch of attracting periodic orbits that already exists for $z_{SN} = 0$ and terminates at a homoclinic bifurcation (HC) for $z_{PO} \approx 0.0036 \in Z_3$. The amplitudes of the attracting periodic orbits are relatively large and roughly even in size. Observe that all of the spikes follow the branch of attracting periodic orbits of the fast subsystem. The square-wave bursting is not as clean as the one shown in Figure 3.1, because the fast subsystem also involves a branch of repelling periodic orbits that emanates from a subcritical Hopf bifurcation (HB).

Figure 4.3(c) shows the pseudo-plateau bursting pattern for $s = -2.09$, which is representative for the pseudo-plateau regime of Figure 4.3(a). The underlying bifurcation diagram of the fast subsystem reflects the conditions discussed in Section 3.2. One of the key conditions satisfied is the absence of attracting periodic orbits for $z = z_{SN}$. Moreover, there is a Hopf

bifurcation (HB) on the upper branch of steady states for $z_{HB} \approx 0.024 \in Z_3$. Furthermore, the upper branch of steady states consists of spiral sinks for $z \in (z_{SN}, z_{HB}) \approx (0, 0.024)$, and spiral sources at least for $z \in (z_{HB}, 2z_{HB} - z_{SN}) \approx (0.024, 0.048)$; this cannot be verified from the figure. Observe how all defining criteria for pseudo-plateau bursting are met in Figure 4.3(c). One distinctive criterion of pseudo-plateau bursting is satisfied, namely, the spikes do not follow any branch of attracting periodic orbits of the fast subsystem. Moreover, the spikes of the burst initially get attracted by the branch of spiral sinks and, hence, decrease in amplitude; then the spikes get repelled by a branch of repelling periodic orbits and the amplitude increases again. Although the spikes do not follow the branch of attracting periodic orbits, the spike amplitudes are larger than those for typical pseudo-plateau bursting, because the organising repellor of the spikes is the branch of repelling periodic orbits rather than the branch of spiral sources (compare with Figure 3.2).

Figure 4.3(d) shows the standard type of transitional bursting pattern for $s = -2.08$, which is representative for the transitional bursting pattern regime illustrated in Figure 4.3(a). Observe that there is a branch of attracting periodic orbits that starts at a fold bifurcation of periodic orbits (FPO) for $z_{FPO} \approx 0.0017 \in Z_3$, and terminates at a homoclinic bifurcation (HC) for $z_{PO} \approx 0.0074 \in Z_3$. Furthermore, there are no periodic orbits of the fast subsystem for $z_{SN} = 0$. As a necessary condition for the standard transitional bursting pattern to transform into pseudo-plateau bursting for sufficiently small ϵ, there is a Hopf bifurcation (HB) on the upper branch of steady states for $z_{HB} \approx 0.0213$; and the upper branch of steady states consists of spiral sinks for $z \in (z_{SN}, z_{HB}) \approx (0, 0.0213)$, and spiral sources at least for $z \in (z_{HB}, 2z_{HB} - z_{SN}) \approx (0.0213, 0.0426)$. All criteria of the standard transitional bursting pattern that we discussed in Section 3.3 are met. The most significant criterion here is that some of the spikes follow the branch of attracting periodic orbits of the fast subsystem and some of them do not. The transitional bursting pattern in Figure 4.3(d) is effectively a pseudo-plateau bursting in disguise. When ϵ is sufficiently reduced, the standard transitional bursting pattern will transform into a pseudo-plateau bursting because the trajectory of the active phase will converge to the branch of spiral sinks and will never follow the branch of attracting periodic orbits.

In summary, all of the three bursting patterns in Figure 4.3 satisfy the conditions and criteria

that we outlined in Chapter 3. We obtained a direct transition between square-wave and pseudo-plateau bursting by changing the position of the z-nullcline. For moderately small ϵ, that is, $0.0001 \leq \epsilon \leq 0.001$, we found that the square-wave bursting regime exists over two s-intervals separated by a single-spike family of periodic orbits. Rather than reducing ϵ further, we consider a different approach. In the next chapter, we investigate the transition between the two bursting patterns when the curve of homoclinic bifurcations of the fast subsystem is shifted to the right in the (z, s)-parameter plane through a change in the value for a.

Chapter 5

Moving the curve of homoclinic bifurcations of the fast subsystem

We found with the previous choices of parameters of system (2.1) and moderately small ϵ, that there exists a single-spike branch of periodic orbits for a relatively large range of s-values in the middle of the bifurcation diagram of the full system. We believe the reason is that the lower saddle-node bifurcation (SN_2) at $z = 0$ and the homoclinic bifurcation (HC) of the fast subsystem are very close to each other in this range of s-values. In this chapter, we change the parameter a from 0.5 to 0.52, which shifts the curve of homoclinic bifurcations further to the right in the (z, s)-parameter plane of the fast subsystem (2.2).

Figure 5.1 shows the two-parameter bifurcation set of the fast subsystem after changing the value of a, and keeping $b = 1$, $\phi = 1$. The black curves represent the curves of the saddle-node bifurcations. The curve of Hopf bifurcations (HB), the curve of homoclinic bifurcations (HC) and the curve of fold bifurcation of periodic orbits (FPO) are coloured red, green and blue, respectively. There are four codimension-two bifurcations in the two-parameter bifurcation set: a degenerate cusp point (DC), a Bogdanov-Takens point (BT), a degenerate Hopf point (DH), and a Belyakov point (B), which are denoted by black dots. The overall structure of the bifurcation set of the fast subsystem has not changed qualitatively by this variation of a. However, note that the curves of homoclinic bifurcations, Hopf bifurcations and fold bifurcations of periodic orbits all have shifted to the right; compare with Figure 2.2. As was the case in Chapter 4,

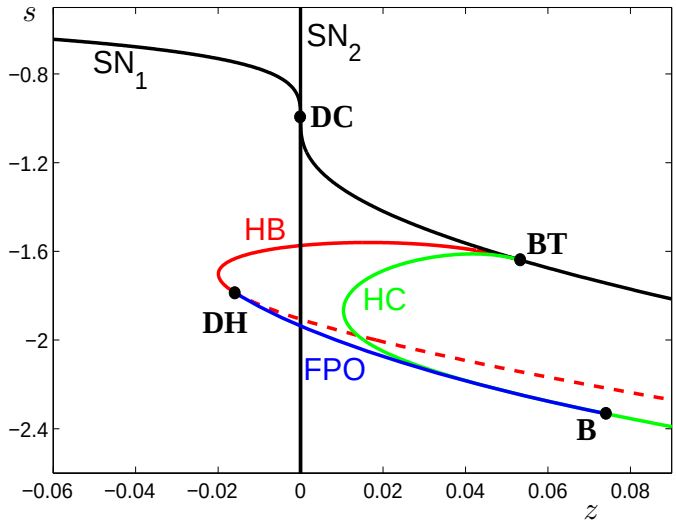

Figure 5.1: Two-parameter bifurcation set of the fast subsystem (2.2). Here z and s are bifurcation parameters, and $a = 0.52$, $b = 1$, $\phi = 1$. Line styles and labels are as for Figure 2.2.

the values $a_1 = -0.3$ and $b_1 = -0.005$ ensure that the equilibrium point of the full system is between the lower saddle-node bifurcation and the homoclinic bifurcation of the fast subsystem (not shown).

Figure 5.2 shows the one-parameter bifurcation diagram of the full system (2.1) with s varying. Here, $\epsilon = 0.001$, $a = 0.52$, $b = 1$, $\phi = 1$, $a_1 = -0.3$, $b_1 = -0.005$ and $k = 0.2$. For this choice of parameters, there is no 1-spike branch of periodic orbits in the middle of the bifurcation diagram, and the square-wave regime occurs within a fully connected family of periodic orbits. Observe how the periodic orbits of square-wave bursting, pseudo-plateau bursting and the transitional bursting pattern are all connected through one single family without the need to make ϵ very small. The spike-adding transition is mediated by a cascade of pairs of saddle-node bifurcations of periodic orbits (SNPs). The transition from square-wave to pseudo-plateau bursting occurs without adding too many spikes. We distinguish the following bursting regimes in Figure 5.2: square-wave bursting (red) occurs for $s \in [-1.936, -1.612]$, pseudo-plateau bursting (green) occurs for $s \in [-2.21, -2.03]$, and the transitional bursting pattern (grey) occurs for $s \in (-2.03, -1.936)$, approximately. The regime of the transitional bursting

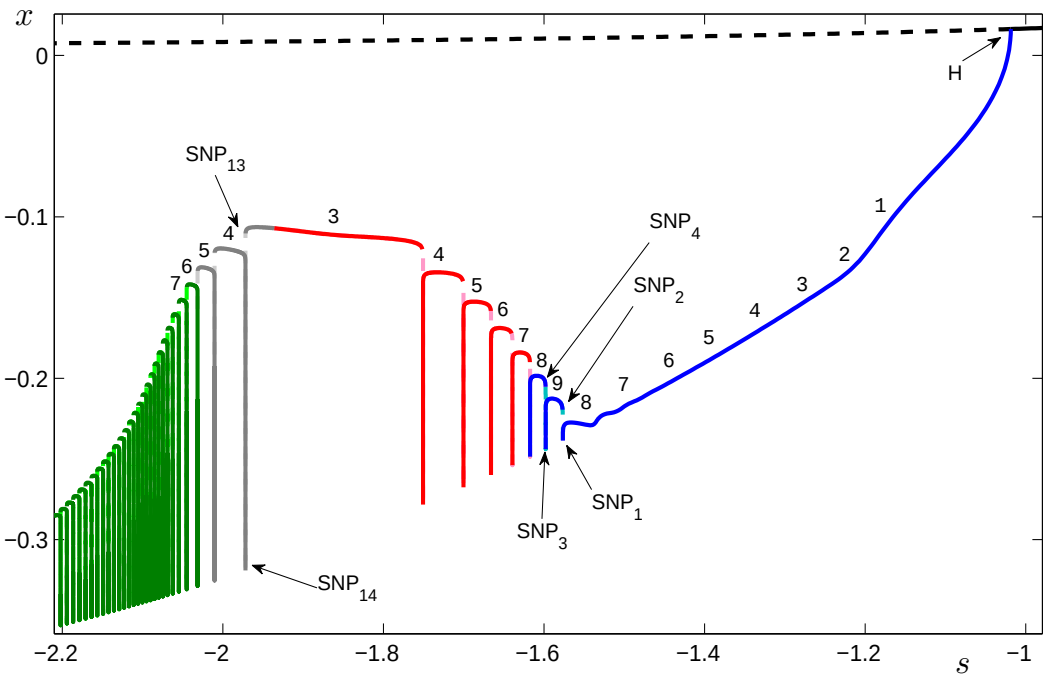

Figure 5.2: Bifurcation diagram of the full system (2.1), with s varying and $\epsilon = 0.001$, $a = 0.52$, $b = 1$, $\phi = 1$, $a_1 = -0.3$, $b_1 = -0.005$ and $k = 0.2$. Line styles and labels are as for Figure 2.10.

pattern is bounded from the right by $s \approx -1.936$, where $z_{FP} \approx z_{SN} = 0$. This regime is bounded from the left by $s \approx -2.03$ where the branch of attracting periodic orbits exists over such a short z-interval that it no longer attracts the trajectory of the active phase. As for the case studies in Chapter 4, the square-wave regime is bounded from the right by $s \approx -1.612$ because the branch of attracting periodic orbits of the fast subsystem terminates at a Hopf rather than a homoclinic bifurcation for the range $s \in (-1.612, -1.56)$. Note that the boundaries of the regimes for the choice $a = 0.52$ are different from those for $a = 0.5$.

Figure 5.3 shows square-wave, pseudo-plateau and transitional bursting patterns for representative values of s in the regimes illustrated in the bifurcation diagram in Figure 5.2. Panels (a), (b) and (c) show square-wave, pseudo-plateau and transitional bursting patterns for $s = -1.80$, $s = -2.05$, and $s = -1.98$, respectively. For all three bursting patterns, the required co-existence interval Z_3 starts from the lower saddle-node bifurcation of the fast sub-

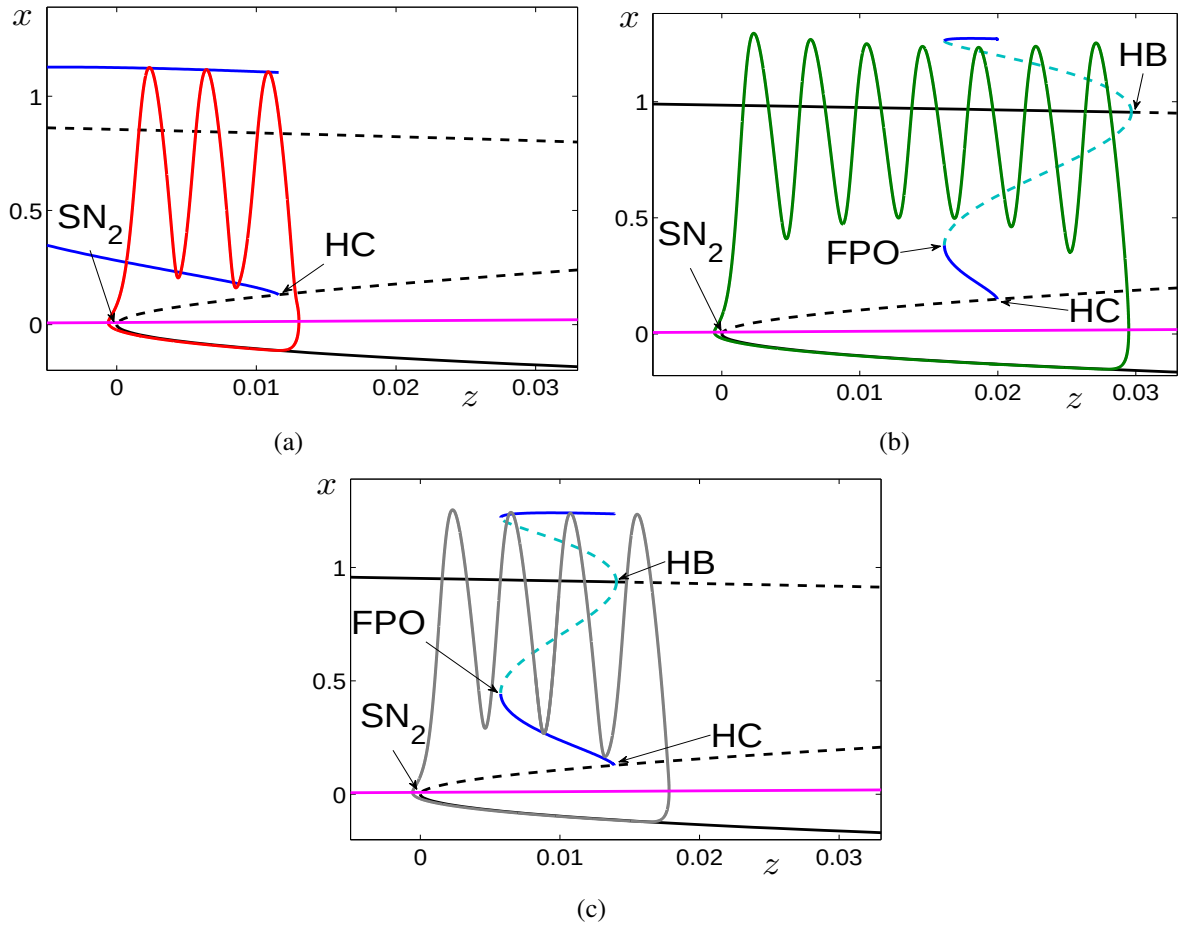

Figure 5.3: The transition from square-wave to pseudo-plateau bursting in the full system (2.1) for the new value of a. Panels (a), (b) and (c) show the bursting patterns overlaid on the corresponding bifurcation diagrams of the fast subsystem for the representative choices of $s = -1.80$, in the square-wave regime; $s = -2.05$, in the pseudo-plateau regime; $s = -1.98$, in the transitional bursting pattern regime, respectively. The values of the other parameters are as for Figure 5.2. Line styles and labels are as for Figure 2.8.

system for $z_{SN} = 0$ and extends past $z = 0.033$. Also for all three cases the lower branch of steady states is stable, and the z-nullcline intersects the curve of steady states on the saddle branch very close to the lower saddle-node bifurcation of the fast subsystem. Note that all conditions and criteria discussed in Chapter 3 are satisfied for all three bursting patterns.

To sum up, we demonstrated our hypothesis which states that we can move from square-wave to pseudo-plateau bursting by varying only s. We obtained a fully connected family of periodic orbits, in which there is a direct transition between the two bursting patterns, by placing the equilibrium point of the full system very close to the lower saddle-node bifurcation of the fast subsystem (SN_2). We can get an even cleaner transition by shifting the curve of homoclinic bifurcations of the fast subsystem to the right in the two-parameter plane of the fast subsystem.

Chapter 6

Conclusions

In this thesis, we studied the transition between square-wave and pseudo-plateau bursting using a generic polynomial model, given by system (2.1). The model is a three-dimensional system of ordinary differential equations where x and y are fast variables and z is a slow variable. We used the approach of freezing the slow variable z to analyse the dynamics of the full system by relating to the corresponding bifurcation diagram of the fast subsystem; refer to Section 1.2 for more detail. By fixing all other parameters of system (2.1), we showed that it is possible to obtain a transition between square-wave and pseudo-plateau bursting via a variation of a single parameter, namely, the parameter s. We described the bursting patterns that arise during this transition in detail. To this end, we proposed characterising criteria and conditions for square-wave, pseudo-plateau and standard transitional bursting patterns for all systems with two fast variables and one slow variable.

6.1 Summary

The characterisation of the different bursting patterns depends mainly on the underlying bifurcation diagram of the corresponding fast subsystem. In Section 2.2, we provided a bifurcation analysis of the fast subsystem (2.2), which exhibits four types of codimension-one bifurcations, namely, saddle-node bifurcations, Hopf bifurcations, homoclinic bifurcations and fold bifur-

cations of periodic orbits (see Figure 2.2). Furthermore, the two-parameter bifurcation set of the fast subsystem consists of four different codimension-two bifurcations: a degenerate cusp point, a Bogdanov-Takens point, a degenerate Hopf point, and a Belyakov point. Due to the polynomial nature of the equations, we were able to find exact formulae for the local bifurcations of fast subsystem, that is, the loci of the saddle-node and Hopf bifurcations, as well as the codimension-two degenerate cusp and Bogdanov-Takens points. Moreover, we found formulae for the sign of the first Lyaponouv coefficient and for the curve where the saddle quantity is zero, which were used to determine the precise location of the degenerate Hopf and Belyakov points, respectively. In that section, we also identified six qualitatively different s-dependent regions of the fast subsystem (see Table 2.1, and Figure 2.7), that are indicative of different bursting regimes of the full system.

The actual bursting patterns that arise and the precise nature of the transition between square-wave and pseudo-plateau bursting mainly depends on the choice of parameters and also on the timescale ratio ϵ. In Chapter 2, we used the original parameter values as given in [32]. In Section 2.3, we examined the behaviour of the full system (2.1) for varying values of s. We did not find a direct transition between square-wave and pseudo-plateau bursting for $\epsilon = 0.01$ (Figure 2.10) and $\epsilon = 0.005$ (Figure 2.11), because of the 1-spike and 2-spike branches of periodic orbits that separate the regimes of the two bursting patterns. However, we found a cleaner transition between the two bursting patterns for $\epsilon = 0.001$ (Figure 2.12). For $\epsilon = 0.001$, the transition route is mediated by isolated branches of periodic orbits (isolas), and the periodic orbits of square-wave and pseudo plateau bursting do not belong to the same family of periodic orbits (Figure 2.12(a)). We observed an overshoot of the trajectory near the lower saddle-node bifurcation of the fast subsystem before jumping up, which we explained by the fact that the z-nullcline intersects the curve of steady states relatively far away from that lower saddle-node bifurcation for that choice of parameters (Figure 2.12(b), (c), (d)).

In order to investigate the precise nature of the transition between square-wave and pseudo-plateau bursting, we proposed in Chapter 3 defining criteria and conditions for square-wave, pseudo-plateau and standard transitional bursting patterns. Here, we restricted to systems with one slow and two fast variables. Using our characterisation, we were able to give a precise description of the different bursting patterns, in terms of both the phenomenological observa-

tion from the time series, and the structure of the underlying bifurcation diagram of the fast subsystem. This chapter complements other attempts to classify bursting patterns [13, 23].

Based on our characterisation in Chapter 3, we were able to predict the best means of changing parameters in order to obtain a cleaner transition between square-wave and pseudo-plateau bursting in our model (2.1). In Chapter 4, we discuss the effect of changing the location of the z-nullcline. By placing the equilibrium point of the full system closer to the lower saddle-node bifurcation of the fast subsystem, we obtained a direct transition between square-wave and pseudo-plateau bursting through a single connected family of periodic orbits (Figure 4.3). Moreover, the trajectories of the bursting patterns did not exhibit any overshoot near the lower saddle-node bifurcation of the fast subsystem. In Chapter 5, we shifted the curve of homoclinic bifurcation of the fast subsystem to the right in the (z, s)-parameter plane (Figure 5.1). As a result, we obtained an even cleaner transition between square-wave and pseudo-plateau bursting via a cascade of pairs of saddle-node bifurcations of periodic orbits. For this choice of parameters, we obtained a single large square-wave regime that is part of the same family as the pseudo-plateau regime.

6.2 Directions for future research

In this thesis, we focussed only on the direct transition mechanism between square-wave and pseudo-plateau bursting. Other transitions are likely to occur via indirect and more complicated mechanisms. We briefly outlined one such mechanism in terms of the structure of the bifurcation diagram of the fast subsystem that would be sufficient to achieve an indirect transition; such a mechanism is not found in our model. It would be interesting to investigate other transition mechanisms using a different model, for example, the model used in [23], which is the polynomial unfolding of a codimension-four doubly-degenerate Bogdanov-Takens point. This model is known to exhibit similar structure in the fast subsystem as discussed in this thesis, but the complete bifurcation structure is not yet known.

In our characterisation of the three bursting patterns, we only considered systems of one slow and two fast variables. Higher-dimensional systems can also exhibit these types of bursting, and may involve other transitional bursting patterns that cannot be observed in three-

dimensional models. Realistic models of neuronal dynamics are often higher dimensional and it would be of interest to explore the existence of transition mechanisms other than the one presented in this thesis.

Pseudo-plateau bursting is a relatively new bursting pattern that has also been classified as a form of so-called mixed-mode oscillation, which is a periodic orbit that exhibits both small- and large-amplitude oscillations [29, 30, 33, 34]. A pseudo-plateau burst has only one large-amplitude oscillation (the silent phase) and an arbitrary number of small-amplitude ones (the active phase). Mixed-mode oscillations require two slow variables [28], but realistic neuronal models often exhibit three different timescales and there are different reduction techniques to analyse such models. In our model (2.1), the variables x and y vary on the same timescale because we set $\phi = 1$. According to our criteria and conditions, we observe a clean pseudo-plateau bursting, despite the fact that there is only a single slow variable.

It would be of interest to explore what happens when we reduce the timescale of y by decreasing ϕ. We did preliminary investigation of this case for $\phi = 0.6$, which makes y slower than x but not in order of magnitude (see Appendix A). Further reducing ϕ can make the variables of the model vary on three distinct timescales. An even further reducing of ϕ can lead the model to exhibit two slow variables (y and z) and only one fast variable (x). Investigation of such cases might give important information about the persistence of square-wave and pseudo-plateau bursting when the timescale ratio is changed significantly; this is beyond the scope of our study is left as an interesting direction for future work.

Appendix A

Changing the timescale ratio

In this Appendix, we present the results from preliminary investigations of system (2.1) after decreasing ϕ, such that the timescale ratio between the variables does not change significantly. Figure A.1 shows the (z, s)-parameter set of the fast subsystem (2.2) with $\phi = 0.6$, $a = 0.5$, $b = 1$. For this choice of parameters, we still consider x and y as fast variables and z as a slow variable. The black curves labelled SN_1 and SN_2 represent the loci of saddle-node bifurcations. The curve of Hopf bifurcations (HB), the curve of homoclinic bifurcations (HC) and the curve of fold bifurcation of periodic orbits (FPO) are coloured red, green and blue, respectively. The two-parameter bifurcation set is qualitatively different from those presented in the earlier chapters, because there exists a curve of saddle-node on invariant cycle (SNIC) bifurcations, which is indicated by the green line segment at $z = 0$ bounded by the two magenta dots. In fact, the curve of SNIC bifurcations arises as the saddle points involved in homoclinic bifurcations (HC) collide with the lower saddle-node bifurcations (SN_2) in the phase space. The full system (2.1) does not exhibit any bursting behaviour for the range $s \in (-2.648282, -1.2558)$, which corresponds to the occurrence of SNIC bifurcations in the fast subsystem. From the conditions on the fast subsystem discussed in Section 3.1, square-wave bursting can occur in the full system approximately for $s \in [-2.648288, -2.648282]$ and $s \in [-1.2558, -1.2435]$. These two small square-wave regimes are separated by the SNIC regime. In both regimes of square-wave bursting, the branch of attracting periodic orbits of the underlying fast subsystem exists for a very small z-range in the co-existence interval Z_3, and ϵ needs to be extremely small in order

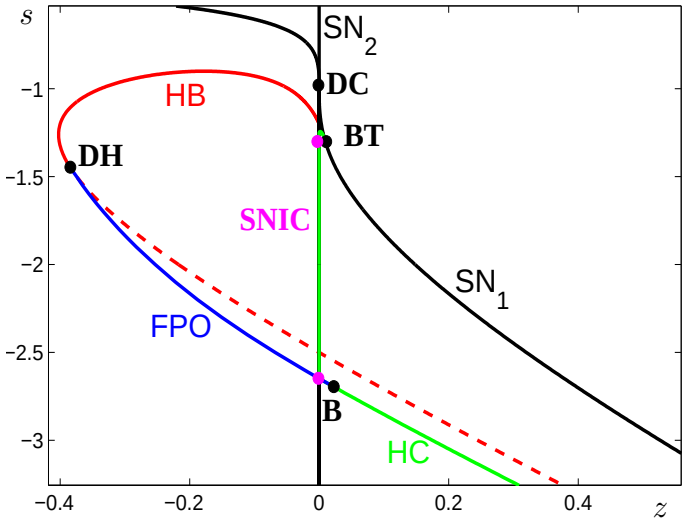

Figure A.1: Two-parameter bifurcation set of the fast subsystem of the polynomial model (2.2), with $\phi = 0.6$. Here z and s are bifurcation parameters, and $a = 0.5$, $b = 1$. The curve of saddle-node on invariant cycle (SNIC) bifurcations is represented by the green line segment at $z = 0$ bounded by the two magenta dots. Other line styles and labels are as for Figure 2.2.

to achieve more than one spike (not shown). From the conditions on the fast subsystem discussed in Section 3.2, pseudo-plateau bursting can occur in the full system for $s < -2.648288$. For moderately small ϵ, the system exhibits pseudo-plateau bursting but not square-wave bursting. We also found the same results for other choices of parameter values that maintain similar timescale ratio between the variables.

In summary, when we reduce ϕ, the square-wave regime of the full system vanishes for moderately small ϵ. Therefore, our method of freezing one slow variable and analysing the dynamics of the system by relating to the underlying bifurcation diagram of the fast subsystem is not the best way to investigate the persistence of square-wave bursting when decreasing the timescale of y. Other reduction techniques might be more useful for such investigation.

References

[1] Baer S. M., Erneux T., Rinzel J., (1989). The slow passage through a Hopf bifurcation: delay, memory effects, and resonance. *SIAM Journal on Applied Mathematics*, **49**(1): 55-71.

[2] Belyakov L. A., (1984). Bifurcation of systems with homoclinic curve of a saddle-focus with saddle quantity zero. *Matematicheskie Zametki*, **36**: 838-843.

[3] Belykh V., Belykh I., Colding-Jørgensen M., Mosekilde E., (2000). Homoclinic bifurcations leading to the emergence of bursting oscillations in cell models. *The European Physical Journal*, **3**: 205-219.

[4] Burke J., Desroches M., Barry A. M., Kaper T. J., Karmer M. A., (2012). A showcase of torus canards in neuronal bursters. *The Journal of Mathematical Neuroscience*, **2**: 3.

[5] Ermentrout G. B., Terman D., (2010). *Foundations of Mathematical Neuroscience*. Springer-Verlag, New York.

[6] Ermentrout B., (2002). Simulating, analyzing, and animating dynamical systems: A guide to XPPAUT for researchers and students, *SIAM*, Philadelphia.

[7] Glendinning P., (1994). *Stability, Instability and Chaos: An introduction to the theory of nonlinear differential equations*, Cambridge University Press, Cambridge.

[8] Ellner S. P., Guckenheimer J., (2006). *Dynamic models in biology*, Princeton University Press, Princeton.

[9] Guckenheimer J., Kuznetsov Y. A., (2007). Bautin bifurcation, *Scholarpedia*, **2**(5): 1853.

[10] Guckenheimer J., Kuznetsov Y. A., (2007). Bogdanov-Takens bifurcation. *Scholarpedia*, **2**(1): 1854.

[11] Guckenheimer J., Kuznetsov Y. A., (2007). Cusp bifurcation. *Scholarpedia*, **2**(4): 1852.

[12] Izhikevich E. M., (2007). *Dynamical Systems in Neuroscience: The Geometry of Excitability and Bursting*. The MIT Press, Cambridge.

[13] Izhikevich E. M., (2000). Neural excitability, spiking and bursting. *International Journal of Bifurcation and Chaos*, **10**: 1171-1266.

[14] Keener J., Sneyd J., (2008). *Mathematical Physiology*. Springer-Verlag, New York, second edition.

[15] Krupa M., Szmolyan P., (2001). Extending geometric singular perturbation theory to nonhyperbolic points—fold and canard points in two dimensions. *SIAM Journal on Mathematical Analysis*, **33**(2): 286-314.

[16] Kuznetsov Y. A., (2006). Andronov-Hopf bifurcation, *Scholarpedia*, **1**(10): 1858.

[17] Kuznetsov Y. A., (1998). *Elements of Applied Bifurcation Theory*, Springer-Verlag, New York, second editon.

[18] MATLAB (2012), *version 8.0.0 (R2012b)*. The MathWorks Inc., Natick.

[19] Mosekilde E., Lading B., Yanchuk S., Maistrenko Y., (2001). Bifurcation structure of a model of bursting pancreatic cells. *Biosystems*, **63**: 3-13.

[20] Neishtadt A. I., (1987). Persistence of stability loss for dynamical bifurcations I. *Differential Equations*, **23**: 1385-1391.

[21] Neishtadt A. I., (1988). Persistence of stability loss for dynamical bifurcations II. *Differential Equations*, **24**: 171-196.

[22] Nowacki J., Mazlan S., Osinga H. M., Tsaneva-Atanasova K., (2010). The role of large-conductance Calcium-activated K^+ (BK) channels in shaping bursting oscillations of a somatotroph cell model. *Physica D*, **239**: 485-493.

[23] Osinga H. M., Sherman A., Tsaneva-Atanasova K., (2012). Cross-currents between biology and mathematics: The codimension of pseudo-plateau bursting. *Discrete and Continuous Dynamical Systems—Series A*, **32**: 2853-2877.

[24] Osinga H. M., Tsaneva-Atanasova K., (2010). Dynamics of plateau bursting depending on the location of its equilibrium. *Journal of Neuroendocrinology*, **22**: 1301-1314.

[25] Rinzel J., (1985). *Bursting oscillations in an excitable membrane model*, in Ordinary and Partial Differential Equations, Lecture Notes in Mathematics, Sleeman B. D., Jarvis R. J. (Eds.), Springer-Verlag, Berlin, **1151**: 304-316.

[26] Rinzel J., Ermentrout G. B., (2003). *Chapter: Analysis of neural excitability and oscillations*, in Methods in Neuronal Modeling: From Synapses to Networks, Koch C., Segev I. (Eds.), second edition, MIT, Cambridge: 251-292.

[27] Stern J. V., Osinga H. M., LeBeau A., Sherman A., (2008). Resetting behavior in a model of bursting in secretory pituitary cells: Distinguishing plateaus from pseudo-plateaus, *Bulletin of Mathematical Biology*, **70**: 68-88.

[28] Szmolyan P., Wechselberger M., (2001). Canards in $\mathbb{R}^3$, *Journal of Differential Equations*, **177**: 419-453.

[29] Teka W., Tabak J., and Bertram R., (2012). The relationship between two fast/slow analysis techniques for bursting oscillations, *Chaos*, **22**(043117).

[30] Teka W., Tabak J., Vo T., Wechselberger M., Bertram R., (2011). The dynamics underlying pseudo-plateau bursting in a pituitary cell model, *The Journal of Mathematical Neuroscience*, **1**:12.

[31] Teka W., Tsaneva-Atanasova K., Bertram R., Tabak J., (2011). From plateau to pseudo-plateau bursting: making the transition. *Bulletin of Mathematical Biology*, **73**: 1292-1311.

[32] Tsaneva-Atanasova K., Osinga H. M., Rieß T., Sherman A., (2010). Full system bifurcation analysis of endocrine bursting models. *Journal of Theoretical Biology*, **264**: 1133-1146.

[33] Vo T., Bertram R., Wechselberger M., Tabak J., (2010). Mixed mode oscillations as a mechanism for pseudo-plateau bursting, *Journal of Computational Neuroscience*, **28**: 443-458.

[34] Vo T., Bertram R., Wechselberger M., (2013). Multiple geometric viewpoints of mixed mode dynamics associated with pseudo-plateau bursting. *SIAM Journal on Applied Dynamical Systems*, **12**(2): 789-830.

[35] Wang, X.-J., (1993). Genesis of bursting oscillations in the Hindmarsh-Rose model and homoclinicity to a chaotic saddle. *Physica D*, **62**: 263-274.